Peoples Democratic Republic of Algeria Ministry of Higher Education and Scientific Research

AHMED DRAÏA UNIVERSITY OF ADRAR

FACULTY OF SCIENCES AND TECHNOLOGY

DEPARTMENT OF MATERIAL SCIENCES

جامعة أدرار-الجزائر

END OF STUDY MEMORY, with a view to obtaining the MASTER'S degree

Option: environmental chemistry

<u>Topic</u>

Study and characteristic of Nitinol Nano-biomaterials alloy prepared by mechanical alloying

---

Presented by: SLIMANI Hafsa

Supervised by: Dr .SAKHER Elfahem   MCB   U. Adrar

BEFORE THE JURY:

President: Dr. ARROUSSI Abdelaziz   MCB   U.Adrar

Examiner: Dr. LAKSACI Hamza   MCB   U.Adrar

University year: 2019/2020

Abstract:

In recent years, smart materials are gaining scientific and technical attention due to their properties, and in particular Nitinol ($Ni_{50}Ti_{50}$), has excellent properties such as mechanical, electrical and chemical.

In addition, in the field of application, Nitinol has great applications such as military science, medical science and aerospace with new applications like smart clothing and drones.

In this study, we will study some properties of microstructure and structure, as well as the influence of the alloy with the introduction to the technical development of the mechanical alloy. With some characteristic devices like, SEM, EDX, we are trying to finish these words.

Keywords: smart materials, Nitinol, mechanical alloy, SEM, EDX.

Résumé :

Ces dernières années, les matériaux intelligents attirent l'attention scientifique et technique en raison de leurs propriétés, et en particulier le Nitinol ($Ni_{50}Ti_{50}$), possède d'excellentes propriétés telles que mécaniques, électriques et chimiques.

De plus, dans le domaine d'application, le Nitinol a de grandes applications telles que la science militaire, la science médicale et l'aérospatiale avec de nouvelles applications comme les vêtements intelligents et les drones.

Dans cette étude, nous étudierons certaines propriétés de microstructure et de structure, ainsi que l'influence de l'alliage avec l'introduction au développement technique de l'alliage mécanique.Avec certains dispositifs caractéristiques comme, SEM, EDX, nous essayons de finir ces mot .

Mots clés : Matériaux intelligents, Nitinol, alliage mécanique, SEM, EDX.

الملخص:

في السنوات الأخيرة، تكتسب المواد الذكية اهتمامًا علميًا وتقنيًا نظرًا لخصائصها، ولا سيما النيتينول ($Ni_{50}Ti_{50}$)، الذي يتمتع بخصائص ممتازة مثل الميكانيكية والكهربائية والكيميائية.

بالإضافة إلى ذلك، في مجال التطبيق، يمتلك النيتينول تطبيقات رائعة مثل العلوم العسكرية والعلوم الطبية والفضاء مع تطبيقات جديدة مثل الملابس الذكية والطائرات بدون طيار.

في هذه الدراسة، سوف ندرس بعض خصائص البنية المجهرية والهيكل، بالإضافة إلى تأثير السبيكة مع مقدمة للتطور التقني للسبائك الميكانيكية. مع بعض الأجهزة المميزة مثل؛ SEM وEDX، نحاول إنهاء هذه الكلمات.

الكلمات المفتاحية: المواد الذكية، النيتينول، السبائك الميكانيكية، SEM، EDX.

Thanks...

Dedication...

To my family who through their prayers and their encouragement, i have been able to overcome all obstacles.

Symbols list

Symbol list

NiTi	nickel and Titanium
Nol	Naval Ordinance Laboratory
Ti	Titanium
Ni	Nickel
Hcp	hexagonal compact
Cc	centered cubic
Ti α	Titanium alpha
Ti β	Titanium beta
a	parameter lattice
Ni α	Nickel alpha
Ni β	Nickel beta
TF	melting temperature
As	austenitic transformation start temperature (austenite start)
Ms (martensite start)	Temperature at the start of martensite transformation
Mf	Martensite finish temperature
GPa	Gigapascals
µm	micro mitre
Co	cobalt
Na	sodium
G*	free enthalpy
V	atomic volume
L	grain size

Symbols list

γs	surface energy of the grain
Ar	Argon
He	helium
N₂	dinitrogen
H₂	dihydrogen
MPa	megapascals
NAVs	Nano air vehicles
h * w *d	height * width *depth
rpm	Rounds per minute
SEM	scanning electron microscopy
EDX or EDS	energy dispersive X-ray spectroscopy.
Fcc	Face centered cubic
C	Carbon
O	oxygen
Cr	Chrom
Fe	iron

Figures list

Figures list

Tables list

Table	Title	page
I.1	**properties of Nitinol**	**-7-**
III.1	**Characteristics of the P7 pulverisette type mill**	**-36-**
IV.1	**Proportions of the elements identified by EDS of the aggregates of particles after 12 hours of milling.**	**-54-**

Table of content

Table of content

Table of content

Table of content

General introduction

Microelectronics emerged as the promising trend in the 1960s, followed by molecular electronics in the 1990s. Molecular electronics work with molecules that act as components of electronic devices. Until recently, the challenge of designing miniature electronic systems integrated into the material structure seemed almost impossible. Nowadays, due to advances in microelectronics and nanotechnology, technologies are available to manipulate structural components as small as 0.1 - 100 nm. Therefore, the two main terms for materials science in the 21st century are "**nanomaterials**" and "**smart" materials** [1].

Shape Memory Alloy (**SMA**) is one class of **smart materials** that has the ability to convert thermal energy into mechanical action. It is commonly used in special engineering applications due to its high energy density and exceptional functional properties. Among the different **SMAs**, Nickel Titanium (**NiTi)** has the best form of memory behavior including high amounts of shape recovery, recovery stress and the superelastic effect are at the origin of these applications in direct relation with the existence of NiTi-austenite (B2) and NiTi martensite (B19`) phases [2].

The nanometric nature of these alloys opens new avenues for the use of these alloys. Several processes have been used to synthesize the nanoscale memory alloys, including precipitation by ion milling, melt spinning, high-pressure twisting, sol-gel technique, etc. Powders have been reported as powder metallurgy, self-diffusing synthesis at high temperature, explosive pressure, and mechanical alloying (**MA**) [3].

Technique mechanical alloying (**MA**) offers new possibilities in producing nanocrystalline powders with metastable structure. Moreover, mechanical alloying is a way of inducing chemical reactions (mechanochemistry), of changing the reactivity of solids (mechanical activation) and of inducing phase transformation in solids [4].

with for example formation of lamellar structures and introduction of defects, followed by a heat treatment , various chemical reactions between co-ground powders or between powders and milling atmosphere, various structural or chemical transformations induced by milling [5].

In this process, the reduction in particle size is observed, which leads to ultra-fine or nanocrystalline grain materials. Due to the very fine particle sizes, nanocrystalline materials exhibit different and often significantly improved properties compared to conventional coarse-grained polycrystalline materials [6].

Milling of a mixture of primary Ni and Ti powders, as well as the amorphous phase, can lead to solid nanocrystalline solutions, NiTi-austenite (B2) and NiTi martensite (B19`) [7]. Therefore, it is very important to characterize the powders obtained by MA in terms of phase formation as well as structural properties and microstructure.

The aim of this paper is to study the effect of milling time on the structural changes and microstructure occurring in mechanically alloyed $Ni_{50}Ti_{50}$ powders mixture. The use SEM characterization is essential in this situation.

This work is gathered in a manuscript structured in 4 chapters.

Chapter one is organized into five main parts. The first concerns definition of nitinol. In the second part, we recall the presentation of pure nickel and titan, and then in the third part we talk about nitinol alloys general, next part explain equilibrium diagram .Then the five part which contains crystallography of nitinol alloy

In the second chapter is devoted to nanomaterials, their properties and synthesis methods, besides mechanical alloying, and applications of NiTi.

To study the effect of the milling conditions on the structural, microscopic, of the samples produced, we have incorporated several characterization techniques: scanning electron microscopy and EDX, and these techniques are presented in Chapter 3.

The experimental results obtained by means of various techniques as well as their discussions are the subject of the fourth and final chapter.

References

[1] **Victor Goldade., Serge Shil'ko., Alexander Neverov:** Smart Materials Taxonomy., Boca Raton, FL 33487-2742.(2016).

[2] **Zhong Xun Khoo.,Yong Liu .,,Jia An., Chee Kai Chua:** Materials 11(4):519 (March 2018).

[3] **Akmal, M., Raza, A., Mudasser, M., Khan., Khan, MI., Hussain, MA**: Materials Science and Engineering C 68 30–36 (2016).

[4] **Suryanarayana S**: Prog Mater Sci ; 46:1. (2001).

[5] **G. Le Ca¨er., R. De Araujo Pont`Es., D. Osso., S. B´egin-Colin., P. Matteazzi**: Journal de Physique IV, 04 (C3), pp.- 233-241,(1994).

[6] **Suryanarayana, C**.: Rev. Adv. Mater. Sci. 18 203-211 (2008).

[7] **Amini, R., Alijani, F., Ghaffari, M., Alizadeh, M., Okyay, AK**: Powder Technology 253 797-802 .(2014)

Chapter I

Nitinol characteristics

Chaptre01: Nitinol characteristics

I.1 Introduction

Nitinol is a word with tow abbreviations **(NiTi and Nol)** . **NiTi** is an alloy composed by 50 % Nickel and 50 % Titanium, and **Nol** from **N**aval **O**rdinance **L**aboratory, which is the place where they first discovered its shape memory aspects in 1960 by w.j Buhler [1]. Today NiTi attracted a great applications area such as military [2], medical [3] engineering [4], and Aerospatiale [5].these due to the unique and important proprieties like the super-elasticity [6] or pseudo elasticity [7], the shape memory effect [8].

I.2 Presentation of pure Nickel and Titanium

I.2.1 Titanium

Pure titanium is a metal in column 14 of the periodic table of elements with two different crystallographic structures stable at low and high temperatures respectively in 882° c. Titanium can crystallize in the Hexagonal Compact (hcp) system(a); Titanium alpha (Ti α) is the most stable form at ordinary temperature. It can also crystallize in the centered cubic system (cc) (b), it is Titanium beta (Ti β) which exists at high temperatures up to the melting point (Figure I.1) [9].

It presents a structure centered cubic parameter lattice a = 3.320 it is very popular in the industry for more than one reason, its density is 40% lower than that of steel but its mechanical strength is important as well as its fire resistance and it has excellent performance at the corrosion. In addition, it is very biocompatible, like gold and platinum [10].
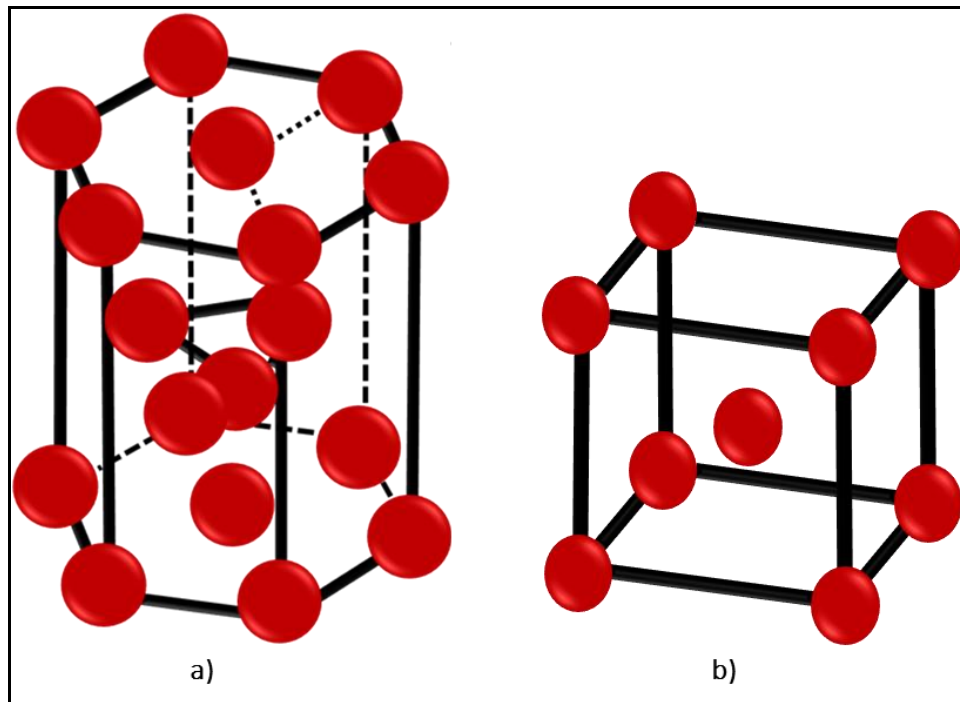
Figure I.1: hexagonal structure of α titanium and β Ti.

I.2.2 Nickel

Nickel is the fifth most abundant element in the earth (2.4%), but far behind the top 4. It is the 24th in the earth's crust, it is a silvery white metal nickel is classified as a transition metal; it is a fairly hard solid body, the hardest of metals after chromium, tenacious, ductile, malleable. There exist under two allotropic varieties, A compact hexagonal structure (hcp) it is (Ni α), this unstable phase and a cubic structure with centered faces (Ni β) stable up to the melting temperature TF = 1450 (Figure I.2) [9].
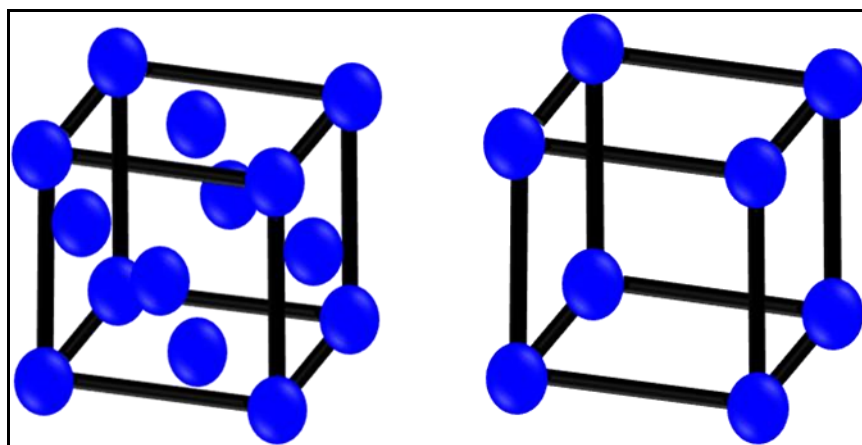
Figure I.2: crystal structure of (Ni β) and structure of cubic.

I.3 Nitinol alloy in general

The origin of the important flexibility of these alloys does not lie in the classical notions of elasticity. Robert Hooke would have been very distressed by the properties of these alloys.

This phenomenon was discovered in 1938, by chance, by Americans or cadmium alloys. It was not until 1963 that nickel-titanium alloy at 50% atomic content (NiTi) is the subject of intensive research and applications [11]. George F. Andresen was the pioneer in orthodontic applications, describing its use in the 1970s [12]. Unite Corporation marketed the first NiTi orthodontic arch under the Nitinol's name. Endodontic applications only appeared much later in 1988. H Walia [13] made the first endodontic files from orthodontic wires .so some properties of this type alloy present in (Table I.1).

Properties	Units	Ti-Ni
Fusion point	°c	1260_1310
Electrical resistivity (As-Ms.)	$\Omega.m*10^{-6}$	0 ,5_1,1
Transition Enthalpy	J/Kg	28000
Young's module	GPa	95
Grain size	µm	20_100
Field of transformation	°c	100_100
Hysteresis (As-Mf)	°c	20_40
Maximum superelatic deformation -Polycristal -Monocristal	%	4 10
Amortization	%	15
Corrosion resistance	\	Excellent
Biocompatibility	\	Excellent

Table I.1: properties of Nitinol [9].

I.4 Equilibrium diagram of Nitinol

NiTi alloys are ordered intermetallic compounds based on equiatomic compo-
sition. This compound exists as the stable phase down to room temperature (Figure I.3)
at low temperatures, the stoichiometric range of NiTi is very narrow and therefore the
alloys often contain precipitates of a second intermetallic phase. The microstructure is
thus primarily single phase, with small amounts of other phases mixed in the matrix
[14].
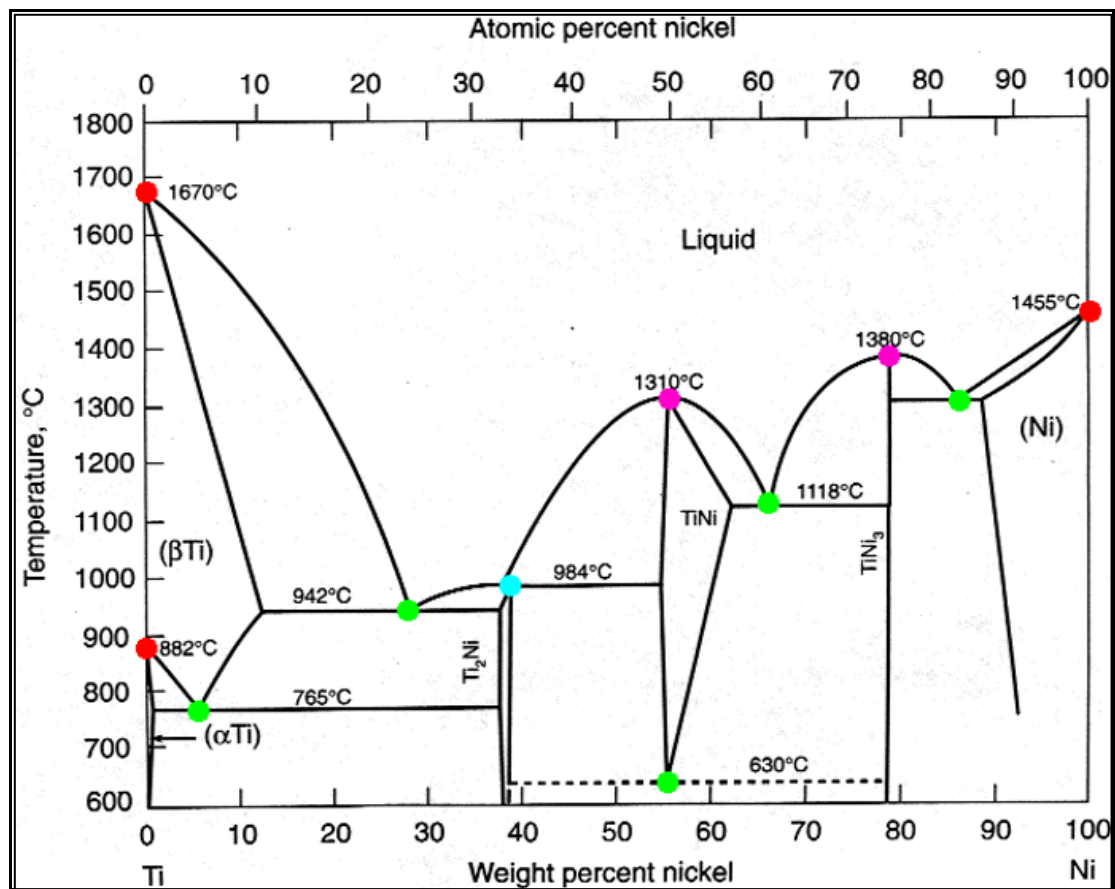
Figure I.3: Equilibrium phase diagram of binary NiTi alloy
[14].

The **Ms.** Temperature of a NiTi alloy is very sensitive to variations in composition, even if it is small (Figure I.4) [15].

When Ni is in excess of the in the equiatomic composition, the surplus is found to be solid in the matrix, which leads to a fall in the transformation temperatures.
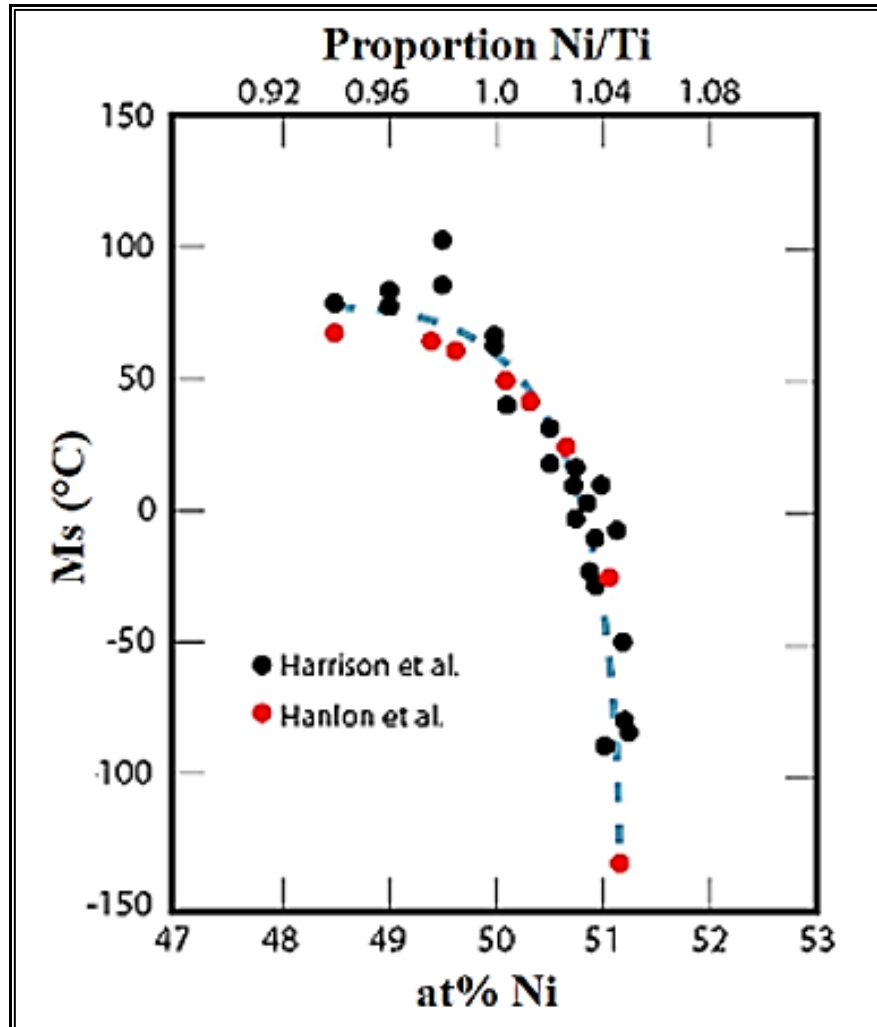
Figure I.4: Evolution of the transformation temperature MS of the NiTi alloy as a function of the atomic composition of Ni [16].

I.5 crystallography of Nitinol alloy

The NiTi alloy exists in different crystallographic forms, which are identified as microstructural phases: austenite (higher temperature or parent phase), martensite (lower temperature or daughter phase) and R-phase (intermediate temperature) [17].

I.5.1 Austenite phase

The NiTi alloys exhibiting the shape memory effect have a high temperature crystallographic structure of cubic type B2 (CsCl) (Figure I.5) this phase, called the mother phase or austenite, is an ordered phase that is stable only for a range composition very close to the equiatomic composition [18].
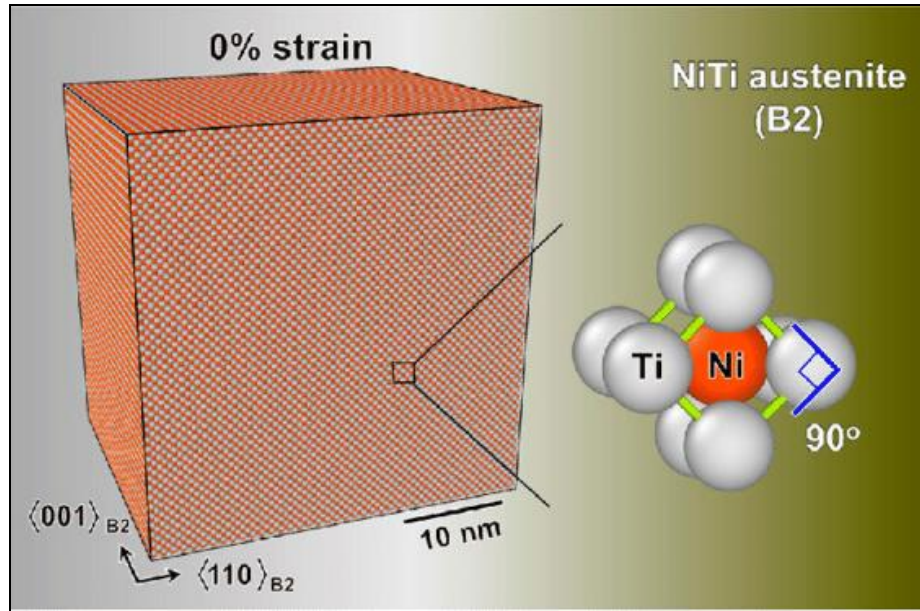
Figure I.5: Single crystal NiTi at the austenite phase (B2) prior to a deformation (at 0% strain). The unit cell structure is of CsCl type [19].

I.5.2 Martensite phase

Several authors (Hehemann, 1971[20], Michal, 1981 [21], Otsuka, 1979, Buhler, 1983) have attempted to determine the martensite structure of NiTi. However, alone and its collaborators, the complete result in neutron defecation, which confirms that the structuring of martensite is monoclinic (Figure I.6).

That the group of spaces is P_{21}/m and which have determined the atomic position, while refining the experimental values of the mesh parameters proposed by others.
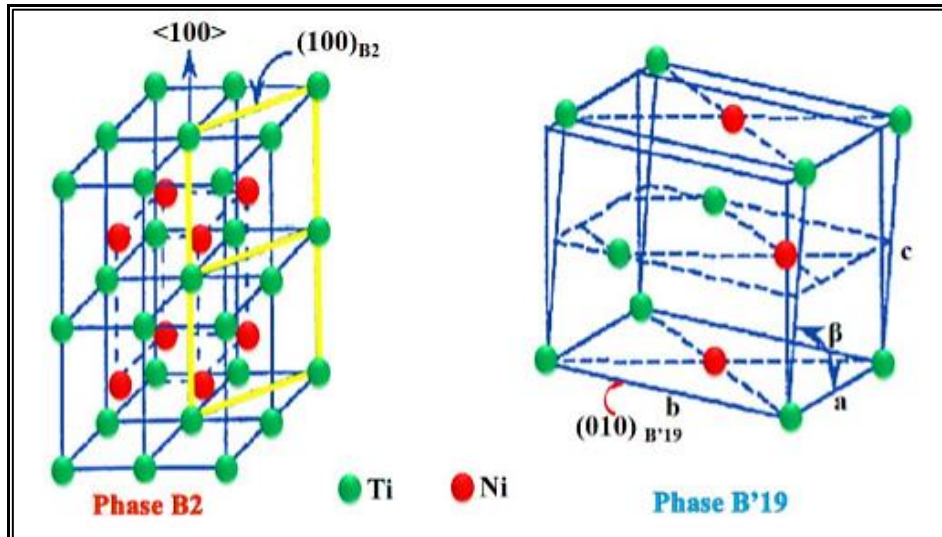
Figure I.6: Presentation of the martensite (B'19) and austenite (B2) structures of the NiTi system.

I.5.3 R-phase

The appearance of martensitic can be preceded by the appearance of a phase R (Figure I.7), the structure of this phase resulting by a distortion from the rhombohedra to a cubic lattice. Those the transformation has the same effect as an elongation of a cubic lattice in the direction of one of the diagonals of the cube with contraction of the perpendicular directions as the change of volume is zero [22].
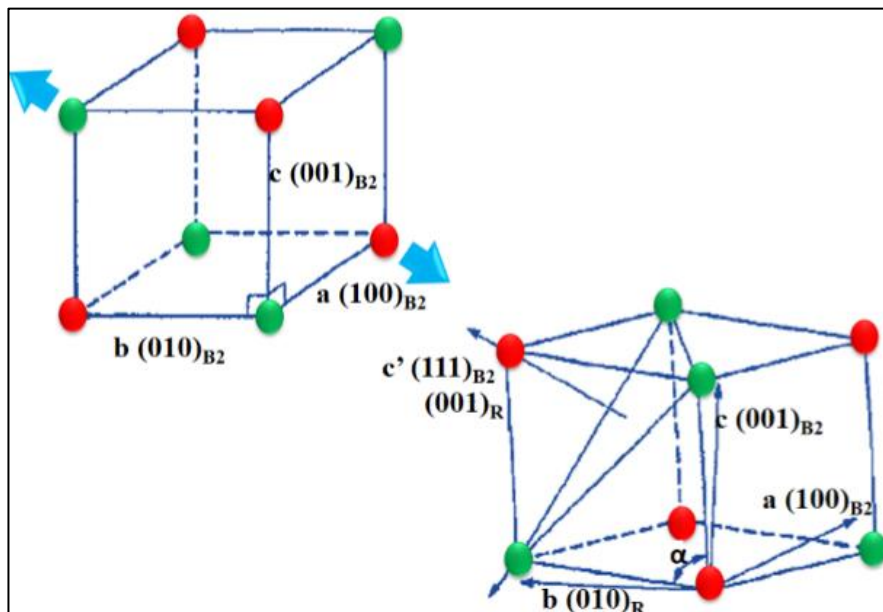
Figure I.7: Structural change of austenite in **R** phase.

I.5.3 Martensitic transformation:

Martensitic transformation is associated with the transformation of the austenite of steels into martensite discovered by Martens in 1879. By extension, this term has been generalized for a certain number of alloys whose transformations have certain characteristics typical of the martensitic transformation of steels, this is the case not only of iron based alloys, but also of alloys or noble metals and titanium base alloys and even certain pure metals (Co, Ti, Na) [23-24].

The martensitic transformation is a displacive transformation of the first order presenting a homogeneous deformation of crystallographic network, mainly constituted by a shear [25].

Both properties result from the phase transformation between an austenitic (parent) phases to a martensitic (daughter) phase (Figure I.8) [26].
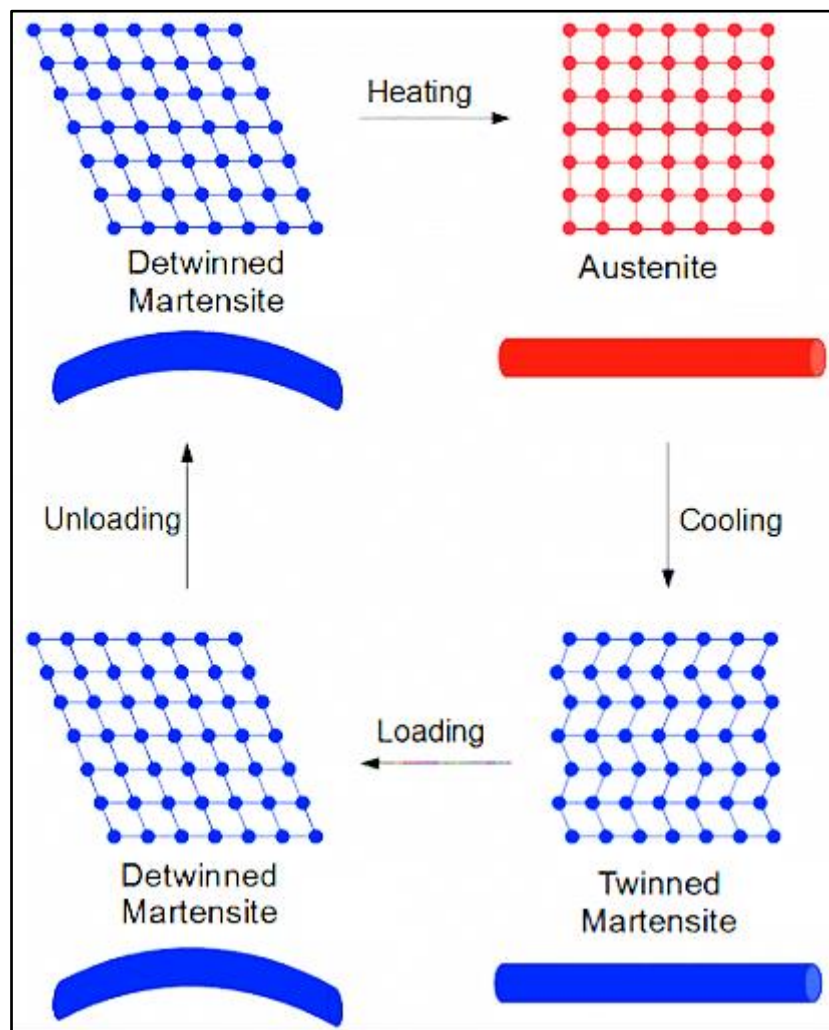
Figure I.8: Martensitic phase transformation (MPT) [27].

References:

[1] **Buhler WJ, Wang FE**: A summary of recent research on the Nitinol alloys and their potential application in ocean engineering. Ocean Enging. 1 (1968).

[2] **C. Naresh., P. S. C. Bose., C. S. P. Rao:** SN Applied Sciences ,vol (314). (2020).

[3] **Min Lu.,Fang Wang., Xiangguo Zeng.,Wenjun Chen.,Junqian Zhang:**Theoretical and Applied Fracture Mechanics.,Volume 105,February (2020).

[4] **Vandreson M., Sergio A., Marcilo A**.: international journal of mechanical sciences. Vol 170 (2020).

[5] **Kaya. H.E.Karaca., M.Nagasako, R.Kainuma:** Materials charterization. Vol 159, January (2020).

[6] **Wang B.,Kang G.,Wenping Wu., Zahou K., Kan Q.,Chao y :** international journal of plasticity**.** Vol 125 (2020).

[7] **Lihong Huang., Xiaoping Yang., Jonahing Gao**: Pseudo-Elastic Analysis with Permanent Set in Carbon-Filled Rubber. 10.1115, (2019).

[8] **ZhiengJ.,P.Oliveira.,SansanAoWeiZhang.,JiangmeiCui.,ShuoYan.,BeiPeng**: Technology., February (2020).

[9] **Sakher El-fahem** : Thèse doctorat en Physique Elaboration et caractérisation de nanomatériaux à mémoire de forme par mécano synthèse – Département de physique. (2019).

[10] **David Cohen :** La Zircone ne suffit pas, le Titane ne meurt jamais : revue de littérature des piliers Ti Base **-**Faculté de chirurgie dentaire .2019

[11] **Civjan S, Huguet EF, De Simon LB**: Potential applications of certain NiTi alloys. J. Dent. Res, 54(1): 89-96 (1975).

[12] **George F. Andreasen**: American journal of Orthodontics and Dentofacial Orthopedics. Vol 96 (1989).

[13] **Walia H, Brantley WA, Gerstein H., J Endod**: An initial investigation of the bending and torsional properties of nitinol root canal files, 14 (1988).

[14] **H Okamoto:** Binary phase diagrams. Metals Park. ASM International (1991).

[15] **Otsuka K., Ren X:** Physical metallurgy of Ti-Ni-based shape memory alloys, Progress in Materials Science 50, 511-678 (2005).

[16] **Farvizi, M**.: Arch. Metall. Mater. 62, 2B, 1075-1079 (2017).

[17] **Thompson SA., Endod J:** An overview of nickel titanium alloys used in dentistry, 33(4):297–310 (2000).

[18] **Bhattacharya K., Kohn R.V:** Symmetry, texture and the recoverable strain of shape-memorypolycristals, Act Materialia 44(2), 529-542, **(1996).**

[19] **Piyas Chowdhury., Guowu Ren., Hussein Sehitoglu:** Simulations, 10 **(2015).**

[20] **Hehemann, R. F., Sandrock, and G. D.:** Scripta Met. Vol 5, p 801-806, (1971).

[21] **Michal, G. M., Sinclair, R**: Actacryst B, Vol. 37, p1803-1807, (1981).

[22] **Laurent, Bataillard, Lausanne, EPFL** : Transformation martensitique multiple dans un alliage à mémoire forme NITI. Thèse N°1518 (1996).

[23] **Guénin G** : Alliages à mémoire de forme Techniques de l'Ingénieur., 10 111 (1986).

[24] **Muller J** : Alliages à mémoire de forme. Matériaux et Techniques., 7(8) (1988).

[25**] L. Jordan, P. Rocher** : Les alliages Nickel-Titane (NiTi). (2010).

[26] **Scott Robertson., Alan R., Peloton, Robert O Ritchie:** Mechanical fatigue and fracture of Nitinol.10 (11) (2012).

Chapter II

Nanomaterials and Nano-Nitinol

Chapter II: Nanomaterials and Nano-Nitinol

II.1 Introduction

The famous physicist Richard Feynman exposed the conceptual foundations of nanotechnology for the first time in 1959. In his lecture "There is a lot of room below", he explored the possibility of manipulating material on the scale of individual atoms and molecules. [1].

Today, nanotechnology contains several fields, it combines biology, chemistry and physics and medicine. Nanotechnology makes it possible to control individual atoms and molecules below the nanometer, up to 100 nm (See figure II.1) [2].
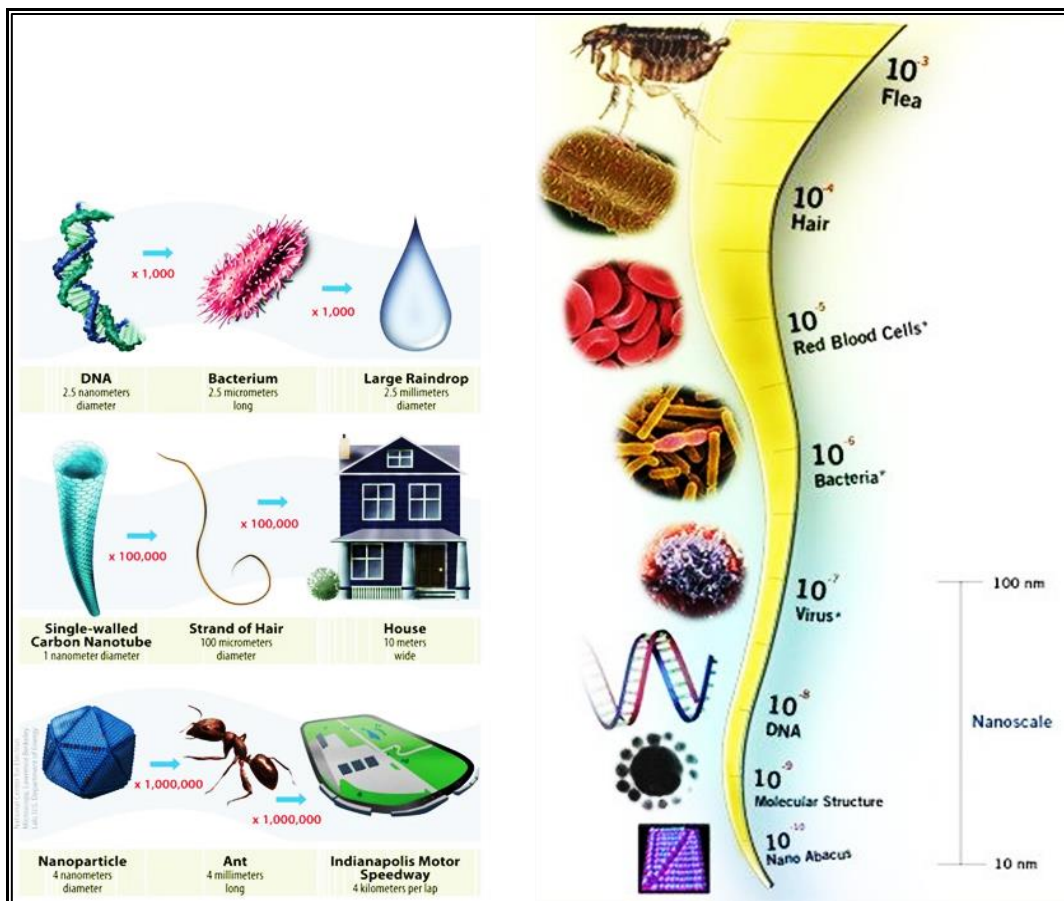
Figure II. 1: Visual examples of the size and scale of nanotechnologies.

II.2 Nanomaterials:

Nanomaterials are mono or polyphase solids whose crystallite size is of the order of a few nanometers (1 to 100 nm) and at least one of their parameters must vary at the nanometric scale (chemical composition, orientation of the network or density atomic), nanaomaterials can be metals, ceramics, carbons, polymers or silicates [3].

II.3. Classification of nanomaterial's:

Nanomaterials can be classified into four families according to their forms of use (Figure II.2):

a) zero dimensional: atomic clusters, filament and cluster assemblies**.**

b) One dimensional: multilayer's same nanowires or nanotubes**.**

- ✓ **Nano wires:** monocrystalline structures with a diameter of a few tens of nanometers and a length, which can range from 500 nm to 10 µm.
- ✓ **Nanotubes:** tubular structures of 1 or 2 nm in diameter and up to 1 mm in length. The best known nanotubes are carbon nanotubes

c) Two dimensional: ultrafine grained over layers or buried layers.

d) Three dimensional: Nanophase materials consisting of equated nanometer sized grains [4].
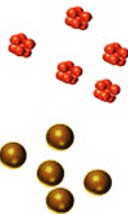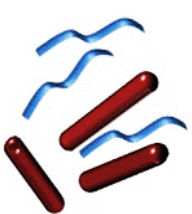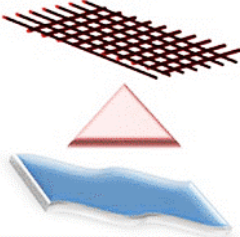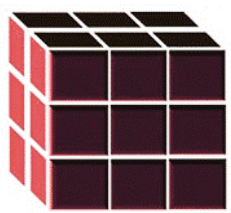
Figure II .2: Schematic representation of various dimensions of nanomaterials [5].

II.4. Nanomaterials properties

Nano scale structures then make it possible to obtain new materials with specific physical, mechanical, electrical, magnetic, optical and catalytic properties or combinations of original properties [6], sometimes differing from the properties of the same material on a different scale.

II.4.1. Physical properties:

Nanomaterials differ from massive materials by reducing the size down to the nanomaterial scale. The very small nanoparticle size leads to a very large specific surface area (Figure II.3), which implies an increase in the number of surface atoms [7].
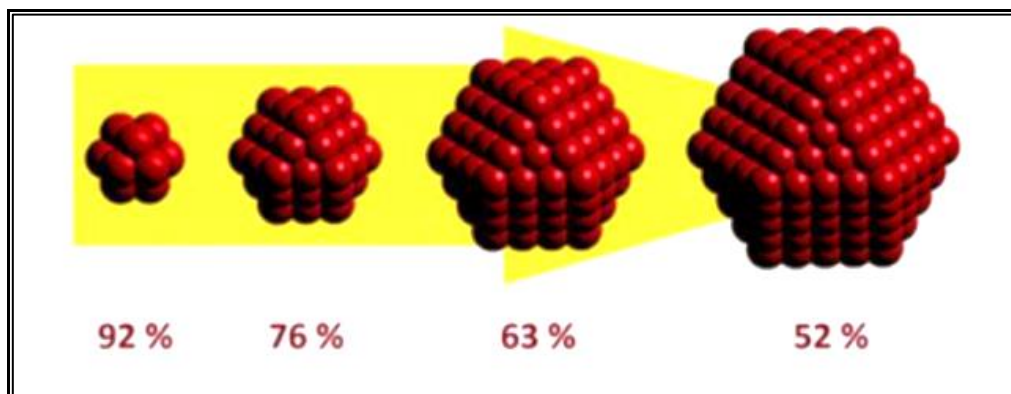
Figure II.3: surface to volume ratio of nanoparticles [8].

In another part, the melting point of nanomaterials is reduced when the grain size is reduced. for example the melting point of gold in its normal size, which reaches 1064 degrees, is reduced to 300 degrees after reducing its grains to about 2,5 nm. [9].

II.4.2. Energies and diffusion:

When the size of the crystallites is of the order of a nanometer, the proportion of atoms located on the surface of the grains becomes large. The thermodynamic and kinetic properties of the materials are then essentially governed by the grain boundaries.

The surface energy ceases to be negligible against the volume of energy; the free enthalpy G should be replaced by a function G * incorporating a surface tension term**:**

$$G * = G - 4\gamma_s \, V/L \, \text{..........................} \quad (II.1)$$

Where **V**, is the atomic volume; **L**, is the grain size; **γs**, the surface energy of the grain depending on its environment. This energy is a function that grows when **L** decreases. [10].

II.4.3. Chemical properties

Nanomaterials have different chemical properties from those of solid materials; different chemical potential and solubility, increased reactivity, notably modification of electro affinity and ionization potential [7].

II.4.4.Optical properties:

The nanoparticles are smaller than the visible light wavelengths (380-780) nm, which improves the optical properties of certain materials (transparency) [4-11].

II.4.5.Mechanical properties:
II.4.5.1 Hardness:

The hardness of a material corresponds to its capacity to resist pressure. The more a metal consists of fine grains, the harder it is. Thus, the nanophase copper is twice as hard as normal coppe [12].

Hall [13]-Petch [14] has been shown that the hardness of metals and nanocrystalline metal alloys prepared by mechanical milling is dependent on the size of the crystallites and the rate of micro deformations (micro-strain) in which the grain size decreases during the milling time [15].

II.4.5.2 Ductility:

The interest in nanomaterials lies in the possibility of combining high mechanical strength and ductility, a microstructural modification of the prepared materials is required that influences the nature of the grain boundaries [16].

II.4.6 Magnetic properties

The influence of the dimension of the crystalline domains has a very important effect on the magnetic behavior of materials with an important technological implication [4]. For example the coercive field that is changed depending on the size of crystalline domains: can be observed an evolution from a magnetically soft material, to magnetically hard and finally to a super-paramagnetic characteristic (figure II.4) [17].
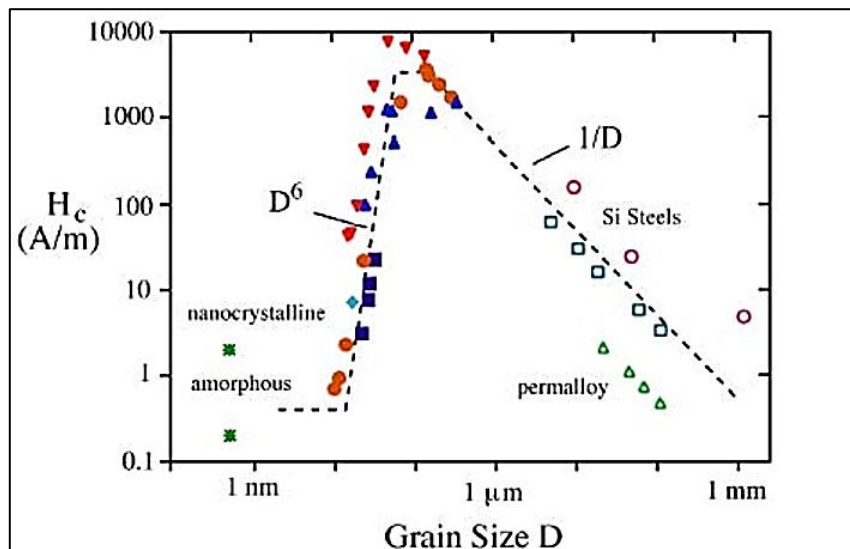
Figure II.4: Modification of the coercive field as a function of the size of the crystal domains [18]

II.5 syntheses of nanomaterials:

There are several techniques, which by their nature can produce materials with small dimensions. Among the techniques used in the production of nanocrystalline materials, we cite:

- Physical vapor deposition, chemical vapor deposition, condensation of inert gases, spraying, plasma process, laser ablation [19].
- Electroplating, rapid solidification, sol-gel process [20].
- Mechanical grinding, mechanochemical synthesis, spark erosion [21].

Nanostructured NiTi alloys can be obtain mechanical alloying [22].

II.5.1 Mechanical Alloying

Mechanical alloying also called mechanosynthesis has been developed in the 1960s, by John Benjamin [23] to produce oxide dispersions (Al_2O_3, Y_2O_3) in nickel alloys in order to strengthen their mechanical properties.

II.5.1.1 Principe

Mechanosynthesis or mechanical alloying is a process used to more or less violently stir a powder and beads contained in a sealed enclosure. Under the effect of collisions, the grains of powder alternately undergo plastic deformations, fractures and welds to each other leading to the formation of nanoscale materials in a metastable state [24].

The reduction of the material into small fragments is obtained by milling; there are three types of fragmentation:

- coarse fragmentation.
- fine fragmentation.
- Ultrafine fragmentation.

Each type of fragmentation corresponds to a specific apparatus. We are only interested in fine fragmentation; this technique consists in grinding two materials A and B together one of the two constituents fragments much more quickly, here substance B. Thus, B reaches its limit fragmentation size before A (figure II.5) [25].
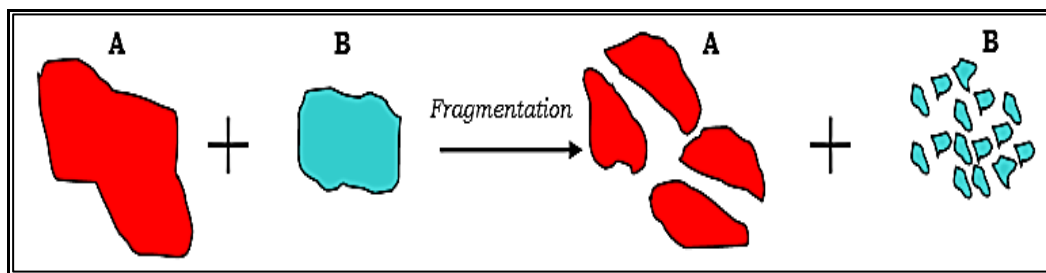
Figure II.5: Diagram of the phenomenon of fragmentation during milling [4].

The fine particles of component B will tend, due to interparticle forces, to stick to the larger particles. The more the milling continues, the more the phenomenon becomes amplified. Different stages of agglomeration will be encountered: the simple welding between

two or more particles, then the stage of coating the particles and finally the stage of agglomeration of the particles between them.

The type of phenomenon observed will depend, among other things, on the duration of the operation and the affinity of the products. Figure II.6shows the evolution of the various agglomeration stages during milling [26].
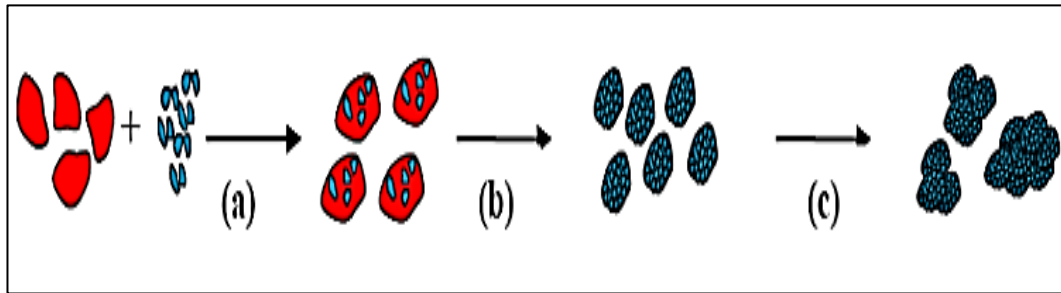
Figure II.6 Different stages of agglomeration during milling:
(a) Welding, (b) coating and (c) agglomeration.

During mechanical alloying, the powder particles trapped between balls or between the balls and the wall of the jar are subjected to plastic deformations, accompanied by hardening phenomena and local temperature rise.

They are fractured and the fragments are then welded together. Typically, around 1000 particles with a cumulative weight of around 0.2 mg are trapped during each collision (Fig. II.7).
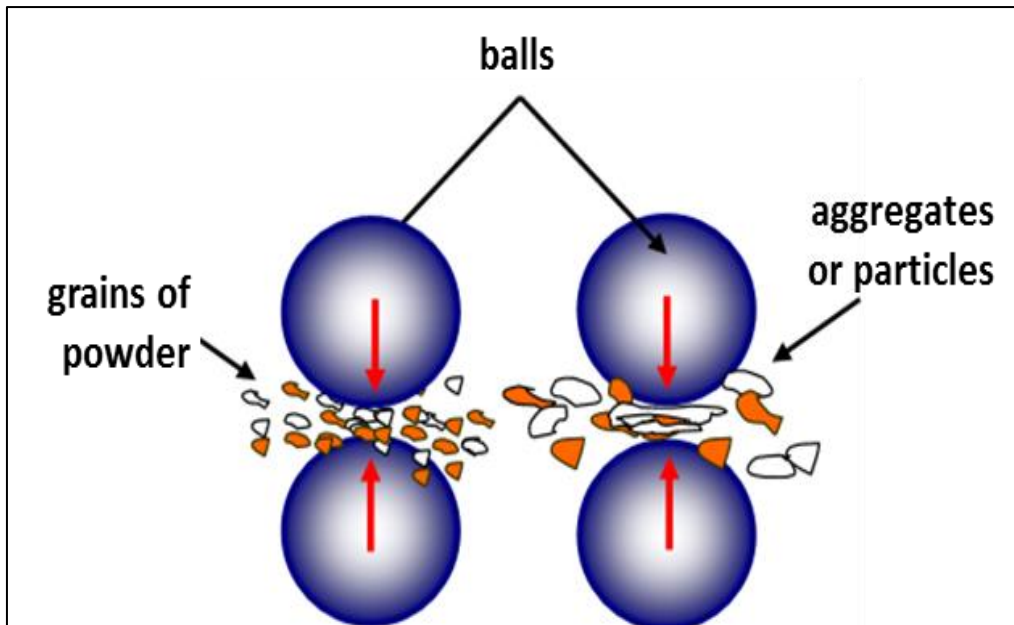
Figure II.7: Principle of mechanical alloying formation of aggregates by mechanical shocks.

II.5.1.2 Experimental grinding conditions

II.5.1.2.1 Nature of powders

The structure, size and shape of the powder particles in the final product are related to the characteristics of the initial powder mixture, such as the chemical nature, the miscibility of the elements, the hardness [27]. There are three types of starting mixtures, which have been described: ductile - ductile, ductile - brittle and brittle-brittle systems [26].

II.5.1.2.2 System ductile - ductile

At the beginning, the particles flatten out and form lamellar structures which weld together. The continued milling then fragments these structures, and the thickness of the lamellae decreases. After sufficiently long grinding, the mixture produced becomes atomic [4].

II.5.1.2.3 System ductile – fragile

In the first stage, the ductile compound is laminated, then incorporating the brittle compound between the lamellae of the ductile compound, then there is uniform

distribution of the brittle compound, at the end it is possible to carry out a mixture at the atomic level [28].

II.5.1.2.4 Fragile system – fragile

In reality, these powders cannot be alloyed by mechanical milling, but under the influence of temperature, it is possible to make a thermal activation accompanied by a reduction in the size of the particles [29].

II.5.1.3 Different types of mills

Different types of milling classified according to the mode of action on the jar or ball, we can cite the following grinders:

The attrition: the balls are set in motion by the rotation of the central shaft on which secondary arms are fixed .the cylinder is fixed (figureII.8).
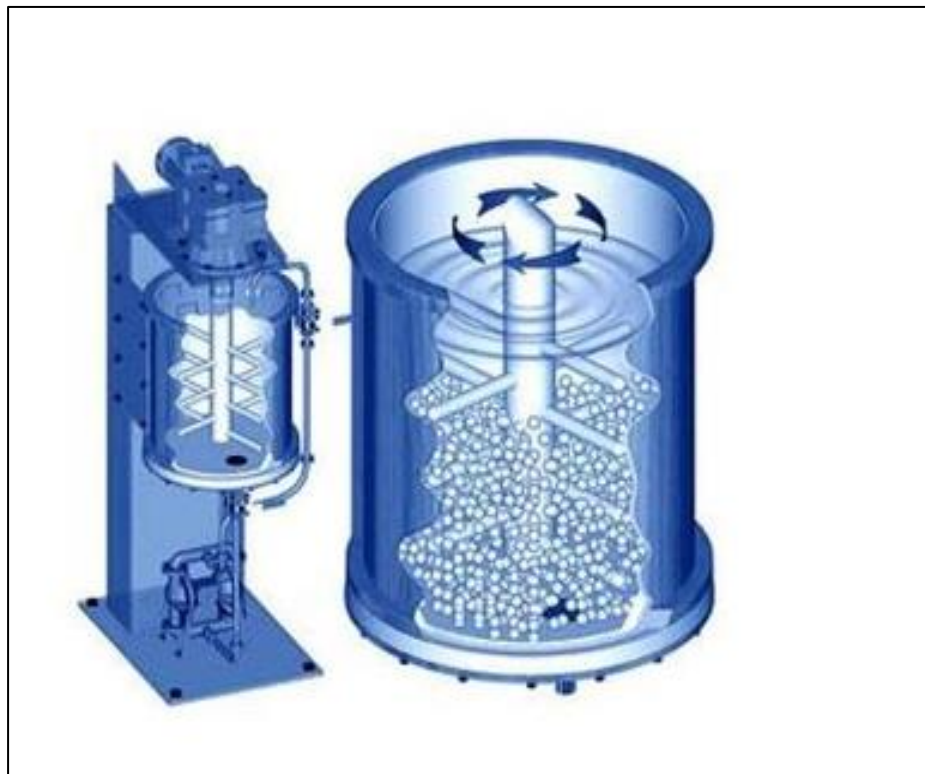
Figure II.8: the milling attrition

The vibrating mill: it consists of a jar in which beads are contained. The jar is moved horizontally forwards, backwards and laterally with a frequency of around 20 Hz (Spex 8000 model) (figureII.9) [30].

Figure II.9: the vibrating mill.

The planetary mill:

In this grinder, ten balls of 1 or 2 cm in diameter are place with the powder in a jar, secured to a disc, which rotates in the opposite direction to it. The milling acts either by impact or by friction. Excluding outside heating, the average temperature of the jar is between 50 ° C and 120 ° C, depending on the speed of the balls, the local temperature rise is between 60 and 300 ° C (figureII.10) [31].

Figure II.10: Fritsch Pulverisette 7 planetary mill.

II.5.1.4.The milling intensity

It depends on the type of mill. When energy is high most obtaining the final product is fast. There are some limitations to the maximum intensity depending on the mill. As in a conventional mill, where the increase in the rotational speed increases the movement of the balls [3].

II. 5.1.5 Milling time

The grinding time is a very important parameter. It is chose so that a stationary state between the phenomena of fracture, welding and re-welding of the powder particles is reached at the end of the process [32].

A milling time pause; this pause is very necessary to avoid sticking to the wall of the mill or to the balls, in a $Fe_{80}Ni_{20}$ powders, the milling temp pause ranging from 3 to 25 h was used [33].

II.5.1.6 ball / powder mass ratio (Ratio Ball Powder RBP)

This ratio depends on the quantity of balls and powders; when the quantity of balls is greater, the mass of powder is minimized to obtain the final product faster and reduce the time required.

It is linked to the number of collisions per unit of time, which increases with the increase in the number of balls. The diffusion process is based on the increase in local temperature, which is linked to the increase in the frequency of collisions. Generally, the ball / powder mass ratio is between 10: 1 and 20: 1[34].

II. 5.1.7Milling atmosphere

Depending on the nature of the atmosphere, grinding can be carried out in a dry (air, Ar, He, N_2 or H_2) or humid environment (organic compounds can be introduced, for example, into the atmosphere of inert gas) [35].

II. 5.1.8 Milling temperature

It has an influence on the process of formation of the final product. A high temperature promotes an increase in the size of the crystallites but reduces their stresses and solubility in the solid state [36].

II.6 New Fields of application of NiTi alloys

II.6.1 Aerospace application

The aerospace industry must minimize the volume and weight of all of their components to minimize launch costs.

Figure II.11: Superelastic Tire, inspired by Lunar Apollo Tires [37].

NASA says that could be a viable alternative to tires on Earth. The Superelastic Tire (FigureII.11), inspired by Apollo lunar tires, uses shape memory alloys (mainly Nickel-Titanium (NiTi) and its derivatives) as load-bearing components. These are capable of undergoing significant reversible deformation (up to 10%) thus allowing the tire to resist an order of magnitude of deformation greater than other airless tires before undergoing permanent deformation [4-37].

II.6.2 Biomedical application

On the orthopedic level, NiTi has been used for bone plates to correct fracture of the spine and scoliosis. In the transition phase, if the shape memory alloy stops changing shape, it can generate stresses up to 700 MPa and these stresses are useful for joining broken bones. In addition, the elastic modulus of NiTi is too close that of the bone material of the human body (figureII.12) [38].

Figure II.12: example for plates fracture of the spine and scoliosis.

Thermally induced elasticity is the main principle behind this stent application of smart materials [39].

Indeed, this stent, once contracted, fits into the artery (Figure II.13). Subsequently, upon relaxation, the superelastic effect forces the artery to return to the original diameter and thus allows the passage of blood [40].
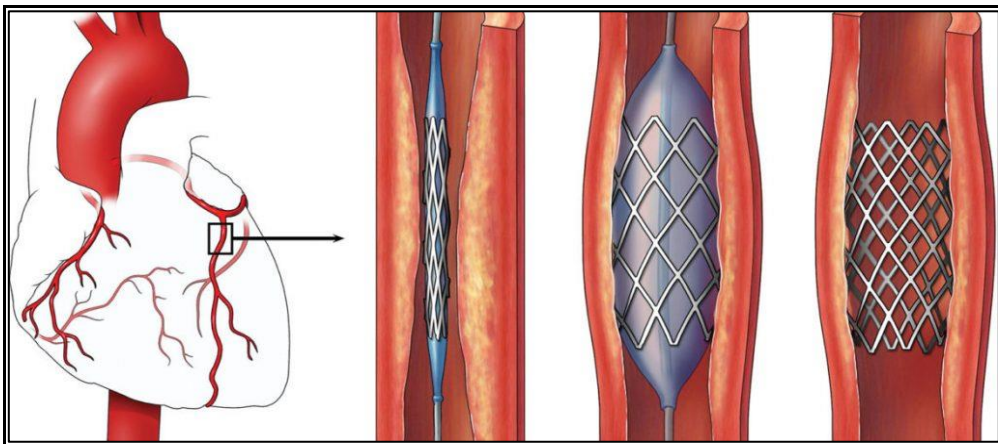
Figure II.13: Coronary artery stent.

Finally, the last example from the biomedical sector is dedicated to medical robots (Nano robots) (figure II.14), which combine their mechanical properties and biocompatibility.
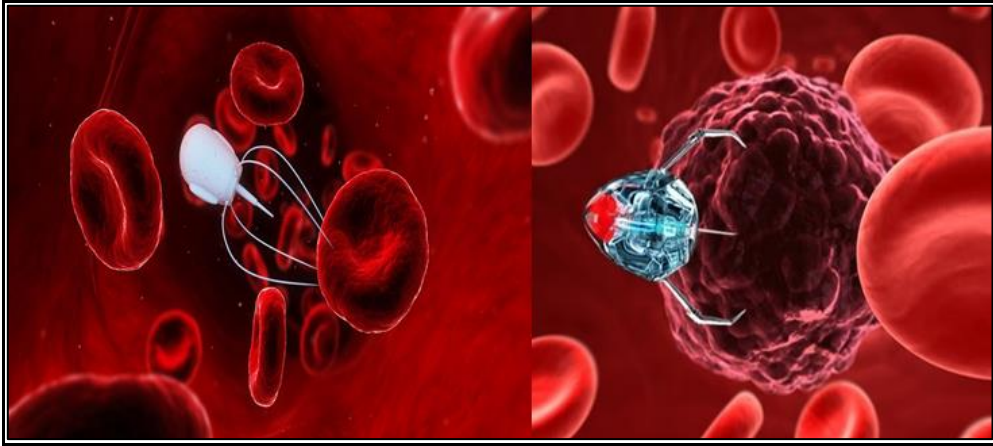
Figure II.14: medical Nano Robot.

II.6.6 Industry application: smart clothes

In the 21st century, clothes are more than ever an interface between the body and the external environment, which is more and more often aggressive, polluted or even toxic, too hot, too cold or too wet, invaded by bacteria and viruses [4].

Today a new fabric has made it possible to manufacture a memory shirt whose fabric rises when it is hot. The fabric is based on Nitinol, a shape memory alloy (SMA) containing nickel and titanium (Figure II.15).

Figure II.15: More functional and smart clothing [41].

II.6.7 Military application

Each type of drone used in urban areas has a mission and a specific technology: large-scale drones carry out military or police missions.

For example kamikaze insect robot that can explode, the mission assigned to these future insects is to fly inside buildings for observation, surveillance, reconnaissance, espionage and even attack missions (a) [42].

In another part, Nano drones (Nano air vehicles (NAVs) are the subject of intense research funded in part by the military (b) (figureII.16).

a)   b)
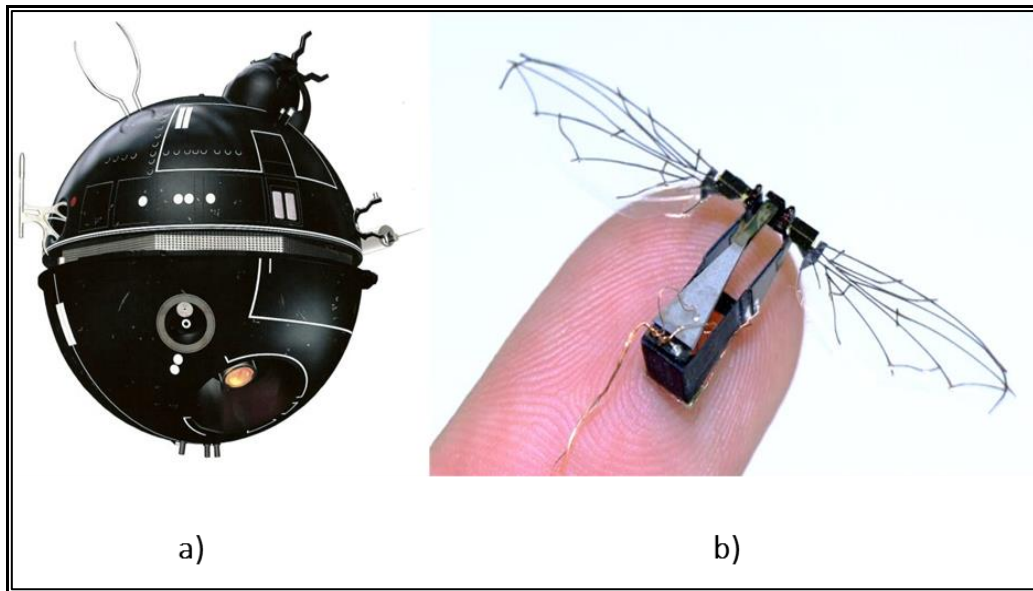
Figure II.16: Example for urban drone [43].

References

[1] **Feynman, Richard P:** There is Plenty of Room at the Bottom; Engineering and Science, 23 (5). pp. 22-36 (1959).

[2] **Freddy C., Carlo Barbante:** Spectrochimica Acta Part B, Atomic Spectroscopy, Volume 86, Pages 3-13. August 2013.

[3] **Ghrieb Sifi :** Elaboration et Etude des Poudres Nanostructurées de FeS2 Obtenues par Broyage Haute Energie- Département de Chimie.2018

[4] **Sakher Elfahem** : Thèse doctorat en Physique Elaboration et caractérisation de nanomatériaux à mémoire de forme par mécano synthèse – Département de physique. (2019).

[5] **Thangarasu Sadhasivam., Kim. Seunghun., HoYoung**:Renewable and Sustainable Energy Reviews. 72:523-534.2017.

[6] **Zhichao Zeng., Yueshan Xu., Zheshan Zhang., Zhansheng Gao., Meng Luo., Zongyou Yin., Zongyou Yin., Zongyou Yin., Bolong Huang., Feng Luo., Yaping Du., Chunhua Yan** .,Chem. Soc. Rev., 49, 1109-1143 ,2020.

[7] **Hamlati Zineb** : étude sur l'élaboration et la caractérisation de l'alliage nanostructure fer-aluminium-vanadium-département construction(2018).

[8] **P. Sonström., M. Bäumer:** phys.chem. vol 13, 19270-19284, 2011.

[9] **Ph. Buffat., J.P. Borel:** American Physical Society**.** Vol. 13, Iss. 6. June 1976**.**

[10] **P. Costa** : Technique de l'ingénieur, M 4026. (2001).

[11] **Yoo, D.J., Lim, D.H., Kang, Y., Lee, C.G., Kang, G.M**.: journal of chemical engineering of Japan, Volume 50(2017).

[12] **Taleb Nawfel.,Boutiara Abdelghani**: Modélisation Cinématique d'un Broyeur Vibratoire (SPEX) pour Nanomatériaux- Institut d'aéronautique et l'étude spatial.(2014).

[13] **Hall, E. O**: proc.phys.soc .Lond., pp 64.747(1951).

[14] **Petch.j**: Iron steel Inst., pp174.25 (1953).

[15] **Loudjani, N., Benchiheub, M., Bououdina, M:** Journal of Superconductivity and Novel Magnetism 29(2016).

[16] **Gherib, M :** Thèse doctorat en Physique Elaboration et caractérisation des matériaux nanostructures et leurs propriétés – Département de physique(2013).

[17] **Herzer, G**.: Handbook of magnetic materials. 10 : 415. (1997).

[18]**G. Herzer**: Mat. Sci. Eng. A133, 1 (1991).

[19] **Cédric R., Vandenabeels.,Stéphane Lucas**: Materials Science and Engineering, R, Reports., Volume 139, January 2020.

[20] **Toubanea, M., Tala ighilb, R., Bensouicia, F., Bououdina, M., Souier, M., Liu, S., Cai, W., Iratni, A**.: Materials Research Express 4(3) 23-35 (2017).

[21] **Evelina C.,Gandrath D.,Alain M.,Tomislav :** Journal of Chemical Education;96(4)2019.

[22] **Nini Ismain Brahim ; Djertli Houssam eddine** : Etude d'Influence des paramètres de broyage dans un Broyeur Planétaire ; Numéro de Thèse 027 (2019).

[23] **J.S. Benjamin**: Metall. Trans2943. 1 (1970).

[24] **BEN ABDESSELAM Djedjiga:** Elaboration de matériaux nanostructurés Fe-Cr par mécanosynthèse et frittage : étude structurale des produits par diffraction des rayons X, Département de Génie mécanique- Université MOULOUD MAMMERI de Tizi-Ouzou(2017).

[25] **Djilali Zidane** : étude de la variation de température en mecanosynthese-Département Aéronautique (2008).

[26] **Loudjani, N.** : Thèse doctorat en Physique, département de physique-université d'Annaba (2015).

[27] **Hamdani Khalida :** Elaborations et caractérisations des couches minces de semi-conducteurs absorbeurs pour les applications photovoltaïques- Département de Physique (2018).

[28] **Koch, C.C., Cavin, O.B., Mckamey, C.G., Scarbrough, J.O**.: Appl. Phys. Lett. 43 1017 (1983).

[29] **Makhlouf, M.B., Bachaga, T., Sunol, J.J., Dammak, M., Khitouni, M** : Metals,vol.6,no.7,articleno.145,(2016).

[30] **Eckert, J., Schultz, L., Urban, K**.: Apl. Phys. Lett. 55: 117 (1988).

[31] **Amara, A., Abdennouri, N., Drici, A., Abdelkader, D., Bououdina, M., Chaffar Akkari F.,, Khemiri, N., Kanzari, M., Bernede, J.C**.: Journal of electronic materials s11664 (2017).

[32] **Zameche Mohamed Ali** : modélisation cinématique d'un broyeur horizontal pou mécanosyntheses- institut d'aéronautique et l'étude spatial. (2015).

[33] **Abderrahim Guittoum**., **Sabrina Lamrani**., **Abdelkader Bourzami**., **Hemmous Messaoud**: The European Physical Journal Applied Physics 65(3)2014.

[34] **C.C. Koch, Annu. Rev**: Mater. Sci, I9-121(1988).

[35] **Kwon, Y. S., Gerasimov K. B., Toon S. K., J**. All. Comp. 346: 276(2002).

[36] **Loudjani, N., Bensebaa, N., Dekhil, L., Alleg, S., Sunol, J. J**: Journal of Magnetism and Magnetic Materials, vol. 323, no. 23, pp. 3063–3070 (2011).

[37] **Gao, X.,Xu, C., Yin, H., Wang, X., Song, Q., Chen, P**: Nanoscale Issue 30, (2017).

[38] **Patrice Berthod:** Advances in Materials Science and Engineering**.,** Vol10. 2016**.**

[39] **D. Stoeckel**: Minim. Invasive Ther. Allied Technol. 9, 2009.

[40] **Busk, S.A**.: Nanostructured titanium dioxide, Department of Mathematics and Natural Sciences Spring (2011).

[41] **http://www.astrosurf.com/luxorion/technologies-futur3.htm**.

[42] **David. Lentink :** micro-et-nano-drone-en-ville**.,** L'université de Wageningen, hollande**.**

[43] **https://laboratoireurbanismeinsurrectionnel.blogspot.com/2011/11/micro-et-nano-drone-en-ville.html.**

Chapter III

Experimental procedure

Chapter III: Experimental procedure

III.1.Introduction

In this chapter, we present the results of the characterization of the mixtures of Ti Ni (x = 50, 50) powders obtained by mechanical milling at high energy.

The morphological, structural and microstructural evolution of the ground powders was followed by scanning electron microscopy

III.2. Summary of samples

The powders of composition $Ti_{50}Ni_{50}$ were produced by mechanical milling with a planetary mill of the P7 pulveriser type from elementary powders of Ni and Ti (see FigureIII.1) [1].

III.2.1. Mill used

The sample to be treated is ground and pulverized by balls in the milling bowl.

The centrifugal forces exerted on the pieces of material to be sprayed and the milling balls are created by the rotation of the milling bowl on its axis and the rotation of the support disc.

The characteristics of the mill .The characteristics of the mill used are presented in Table III.1 [2].

Dimensions (h * w *d)	36x 40 x 58 cm (height x width x depth)
Weight	44 kg (Net) 61 kg (Gross).
Sound level	The noise level is around 74dB (A). The noise level varies according to the speed of rotation, the grinding process in progress (characteristics of the materials being processed, type of balls, etc.)
Voltage	AC voltage 100-240V ± 10%. Transient overvoltages falling within admissible category II.
Current intensity	8.8 A (115V) / 3.7 A (230V)
Power consumption	1300 W
electrical safety devices	2x10 A T
Materials to be treated	5 mm Size of the pieces for hard materials 2 * 35 ml Maximum quantity

Table III.1: Characteristics of the P7 pulverisette type mill [2].

Figure III.1: Fritsch Pulverisette 7 planetary mill.

III.2.2.Conditions for preparation

Elementary powders of high purity Ti (~ 150 μm, 99.97%) and Ni (~ 45 μm, 99.99%) (Aldrich) were mixed in appropriate proportions in order to obtain the composition $Ti_{50}Ni_{50}$ (% at).

Mechanical milling was carried out under an argon (Ar) atmosphere using a Fritsch Pulverisette 7 planetary mill equipped with a hardened steel flask (80 ml) and 15 mm diameter balls also made of hardened steel.

To avoid contact between the outside atmosphere and the powder, during mechanical treatment.

It is important to note that this operation took place in a glove box (figureIII.2) and required an initial primary pumping and an injection of neutral gas (argon) [3].

FigureIII.2: Image of a glove box [3].

The disc rotation speed was $\Omega = 400$ rpm. The mass ratio of beads to powder was 23: 1.

To avoid an excessive increase in temperature, the milling times of 30 minutes were alternated with equal rest periods.

The powders were ground for several periods; 0, 1, 3, 6 and 12h.

III. 3. Characterization of powders

Several techniques have been used for the characterization of ground powders. Changes in the morphology of the powder particles (changes in the size, shape of the powder particles and their distribution) were monitored by scanning electron microscopy (SEM).

III.3.1 scanning electron microscopy

The SEM uses an electron beam instead of light exploiting the wave-particle duality of electrons, this beam is produced to accelerate (1 to 20 kv) on a samples thanks to the lenses (figureIII.3).

The samples then emit secondary electrons, which are then detected; the number of electrons detected depends on the variations in the surface of the sample by scanning a beam and detecting the variation in the number of scattered electrons, we can reconstruct the surface topography.

Figure III.3: scanning electron microscopy, SEM.

References

[1] **Sakher El-fahem** : Thèse doctorat en Physique Elaboration et caractérisation de nanomatériaux à mémoire de forme par mécano synthèse – Département de physique. (2019)

[2] **Fritsch Gmbh** : Laboratory Equipment manufacturing, Industries 8, D 55743, 06/2007.

[3] **Ghrieb Sifi :** Elaboration et Etude des Poudres Nanostructures de FeS_2 Obtenues par Broyage Haute Energie- Département de Chimie.2018.

Chapter IV

Results and Discussions

Chapter IV: Results and Discussions

We propose in this chapter the results and discussions of SEM and EDX.

IV.1. Morphological and microstructural study

IV.1.1. Morphology of powder particles

The evolution of the morphology of the powder particles (the size, shape of the particles and their distribution) as a function of the milling time were determined by scanning electron microscopy (SEM).

The measurements of the chemical composition of the powders for the different milling times were determined by energy dispersive spectroscopy (EDS) at 20 kV.

IV .1.1.1. Morphology of pure elements

Before milling, the Ni particles, varying in size from (2 to 110) µm, are characterized by irregular contours. Note that Ni particles are smaller than Ti particles (20 - 250µm).

We also note the existence of agglomerates, representing the grouping of several fine particles due to the method of preparation.

The samples also contain white filaments, which may come from offcuts from the apron or from the component threads of the carbon protection adhesive used as the backing of the samples [1].

The morphology of titanium powder, as we mentioned previously, the particle sizes are between 20 and 250 µm, and we note that there are two types of particles, the majority of which are characterized by irregular contours, and intermixed and rounded in shape [2].

The second type of particles (minority) have the shape of cubes (crystals) and can represent the cubic centered structure (cc); it is beta titanium (β-Ti) which exists at high temperatures (unstable).

IV .1.1.2. Morphology of milled powders

The evolution of the morphological form and the corresponding particle size distribution of the powders obtained after 1, 3, 6, 12 hours of milling time is presented in figure IV.1.

Morphological changes of $Ti_{50}Ni_{50}$ powder particles occurring during mechanical milling of the fcc -Ni and hcp -Ti starting mixture may be related to the difference in the mechanical properties of metals [1].

It can observed that the morphological changes are already significant just after 1 hour of milling (Figure IV.1, 2).

The particles are flattened by the plastic deformation caused by the progressive forces induced by the ball-powder-ball and ball-powder-jar contacts.

This is also because Ni and Ti are ductile materials, which leads to increasing particle size besides a few small particles produced [3].

With the progression of milling, where we observe both the dominance of fracturing over welding and the increase for phase, the brittleness of the powders increases.

The size of the particles is significantly reduced, and their spherical equiaxial morphology increasing.

After a certain milling time, a balance is reached between the welding speed, which tends to increase the average particle size, and the fracturing speed, which tends to decrease the average particle size [4].
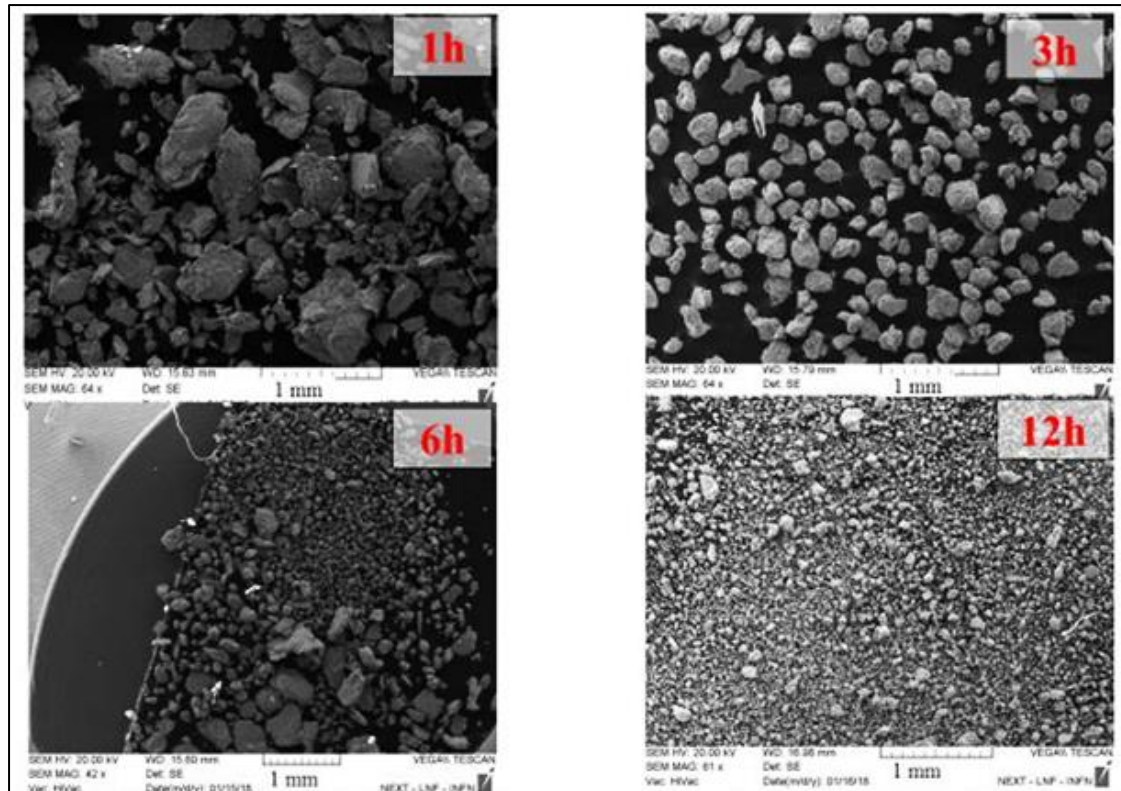
Figure IV.1: Morphologies of $Ni_{50}Ti_{50}$ powders for different milling times: 1, 3, 6 and 12h.

We notice in the powder ground for 1 hour (Figure IV.2), a "lamellar" structure, made up of alternating layers of Ni and Ti.

We focused on a particle with a magnification of 50 and 10 µm, which showed many phenomena, such as adhesion of layers, fracturing and cracking, with the existence of holes from 0.5 to 1 µm and small particles of the same size which may belong to these holes [5].
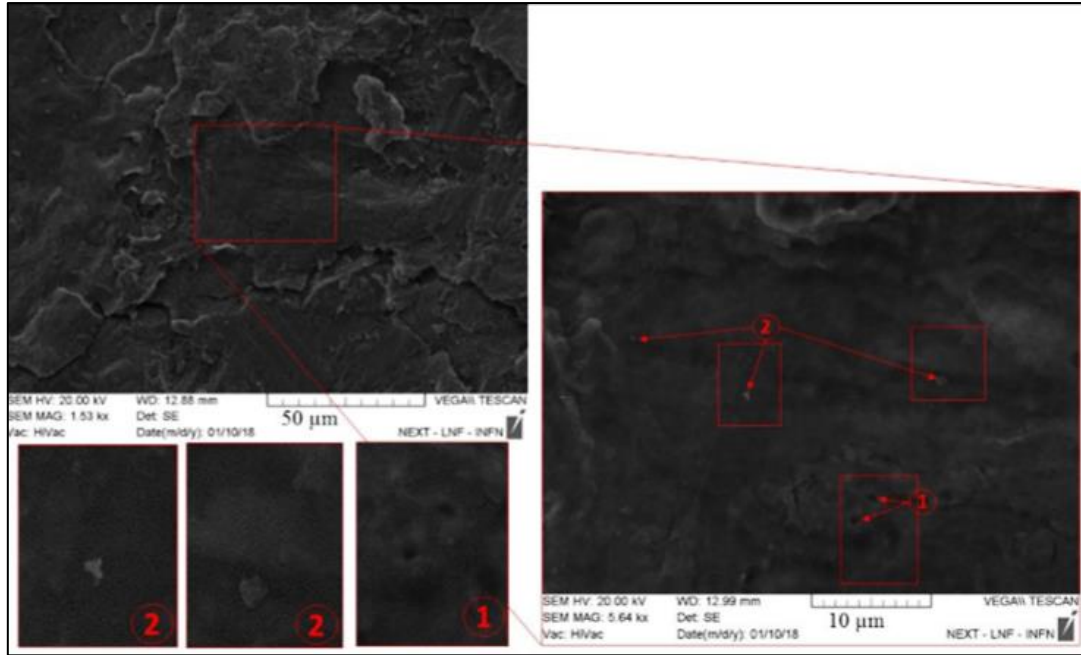
Figure IV.2: Morphology of a powder particle after 1 hour of milling.

Figure IV.3 shows, after 3 hours of milling, the two phenomena of intensive fracturing (Figure IV.3 (a)) and cold welding (Figure IV.3 (b)), due to repeated collisions (balls - powder-beads and beads-powder-bowl wall) [5].
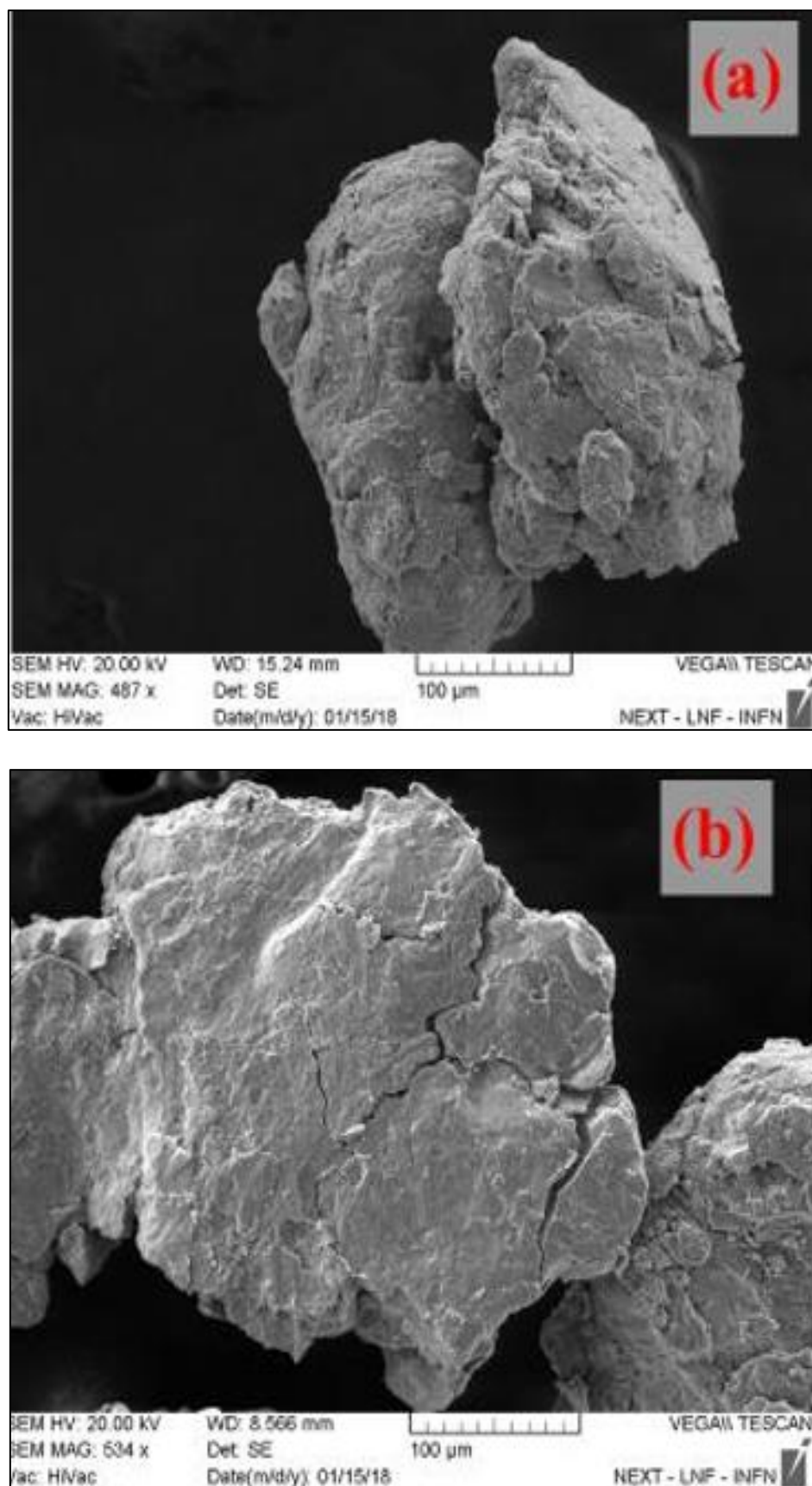
Figure IV. 3: SEM micrograph of the powders ($Ni_{50}Ti_{50}$) showing the cold welding

(a) and the fracture (b) after 3 hours of milling.

After 6 hours of milling, the presence of different types of particles is noted. Figure IV.4 showing the phenomenon of cold welding (sandwich) which shows the formation of thin layers of the initial elements.

We also find particles which appear with facets of different angles (whose size is less than 100 µm) and whose pointed ends can be crystallized and will increase in number with the progress of milling (Figure IV.4).

This figure shows fractured particles that result from impacts between beads-powder-beads and beads-powder-bowl, which may be the reason for the production of small crystalline particles as the milling progresses [1].

This also explains the appearance of another type of particles, in agglomerates of small particles (Figure IV.4). The same observations are to be reported after 12 hours of milling.
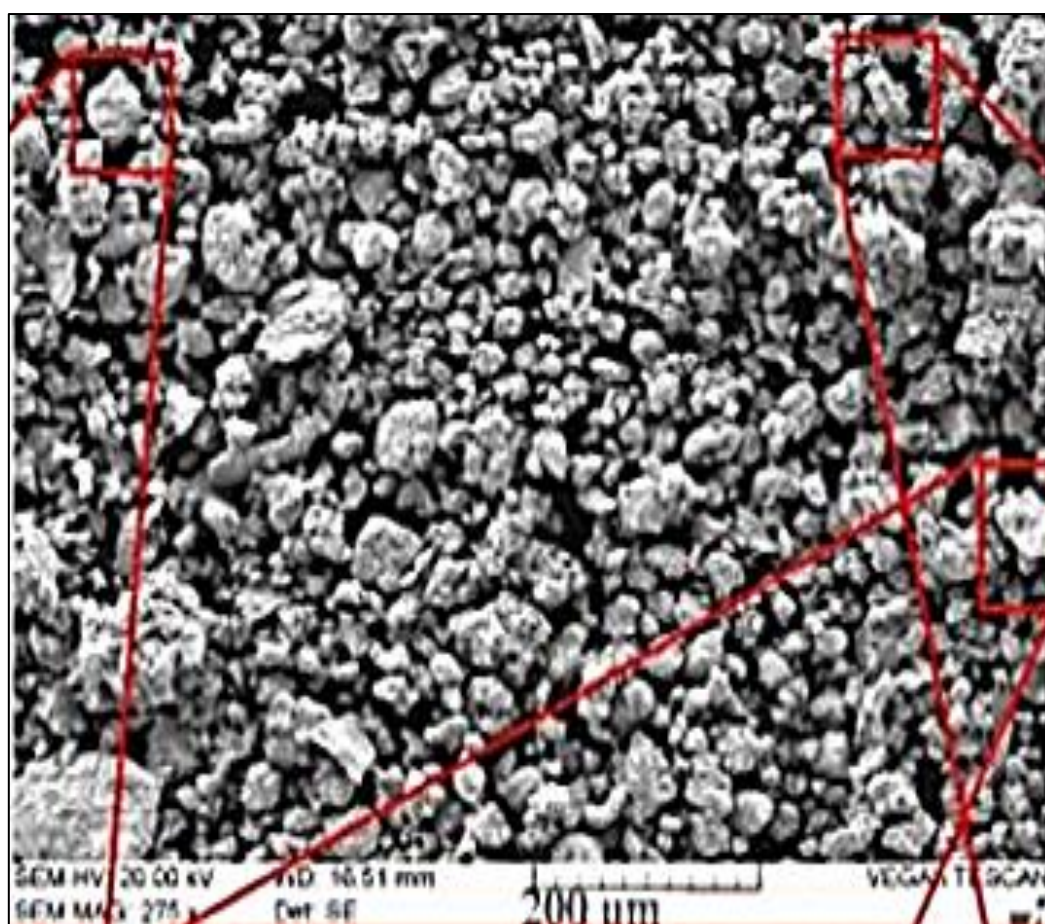

Figure IV.4: Morphology of powder particles after 6 hours of milling: the phenomenon of cold welding, fractured crystalline particle and agglomerates of small particles.

46

After 12 hours of milling, we have the same observations. It should be noted that these results are in agreement with the results of XRD which show that the amount of crystalline phases of martensite and austenite which begins to appear and to increase from of 12 hours of milling.

IV.1.2. Analysis of chemical composition by EDX

The main objective of this part is to ensure that a homogeneous distribution of the elements Ni and Ti was obtained after milling.

By this analysis, we were able to verify that the chemical composition of the powder particles varies little from one sample to another.

This part also shows the mapping spectra for the elements Ni and Ti and the elements that can appear due to contamination by the milling tools like Fe, O, Si, Cr and C, in the $Ni_{50}Ti_{50}$ system for powders obtained after 1, 3, 6, 12 hours of milling time.

After 1 hour of milling (Figure IV.5), we analyzed the different elements and this is based on the analysis results of the SEM scanning microscope.

One can note the presence of Ni and Ti, which are mainly localized on the analyzed powder particles, while the elements O and C are mainly located on the carbon adhesive tape, which is used to fix the samples.

We find the elements Cu and Al placed on the sample holder [6].

Figure IV.5: Map of the distribution of $Ni_{50}Ti_{50}$ powder elements after 1 hour of milling.

After 3 hours of milling, the distribution of the elements Ti, Ni and O on the powder grains is presented in Figure IV.6.

It can be seen that the flat particles have an irregular distribution of Ni and Ti on some particles while it appears uniform in other particles.
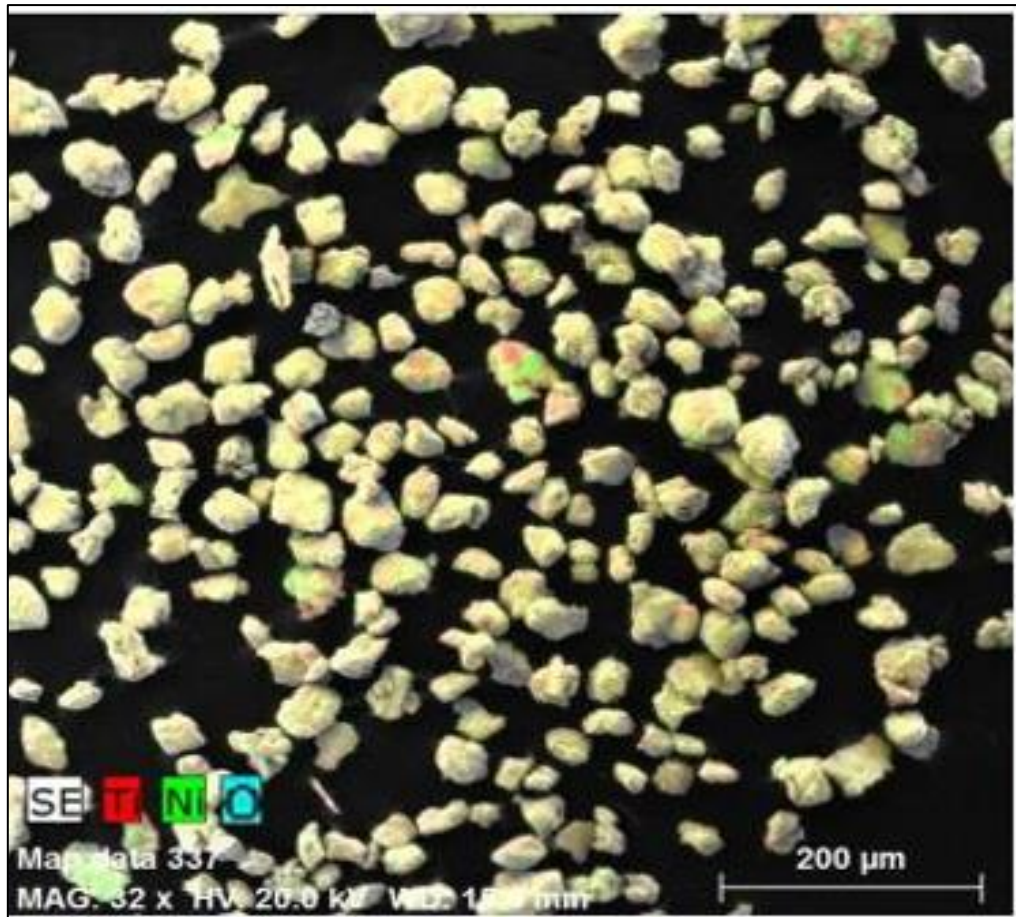
Figure IV.6: Map of the distribution of $Ni_{50}Ti_{50}$ powder elements after 3 hours of milling.

Figure IV.7 presents the mapping of the phenomenon of fracture and / or welding of a group of small particles and shows that the distribution of Ni and Ti is relatively homogeneous but with the clear existence of clusters of each of these elements. . The presence of oxygen is mainly due to the carbon adhesive.
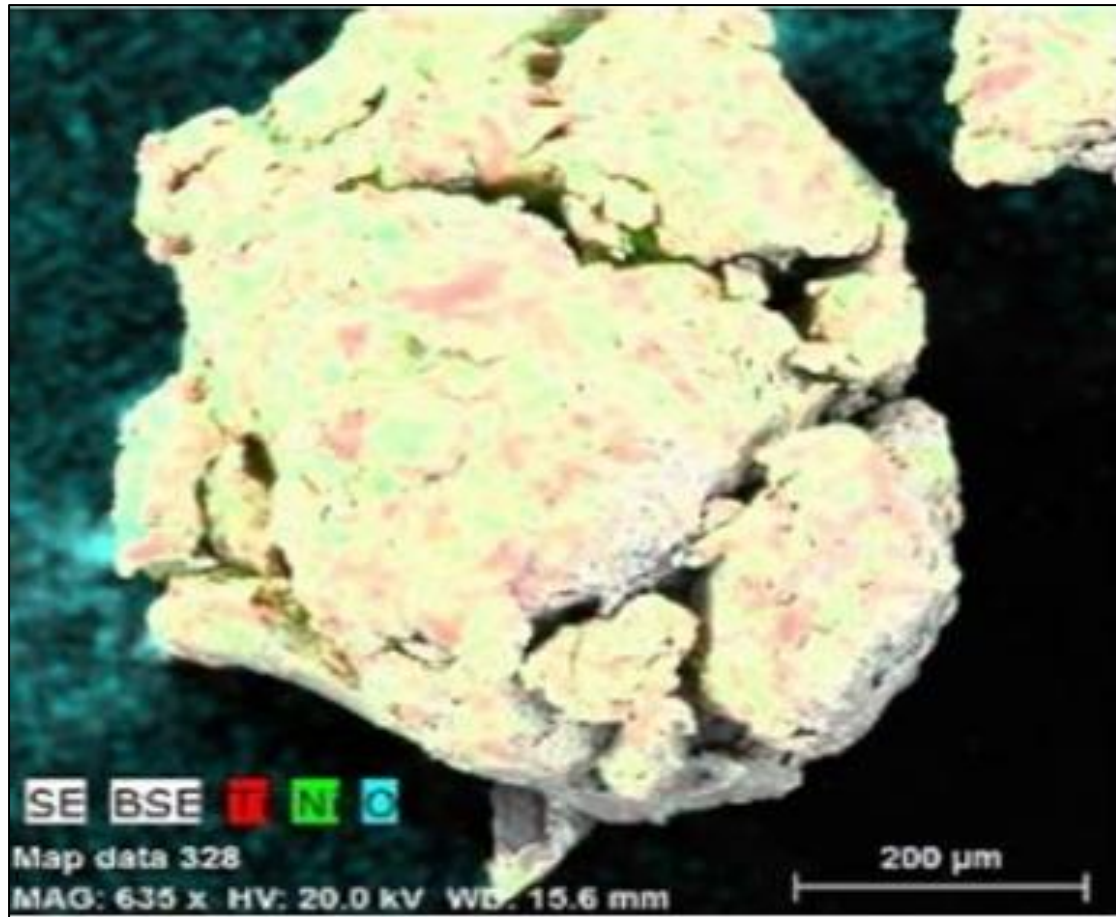
49

Figure IV.7: Mapping of the distribution of elements on a particle after 3 hours of milling.

By focusing on another type of particles (~ 400µm) of the powder ground at 3 hours (Figure IV.8), we observe that there is an inhomogeneity of the distribution of Ni and Ti and the presence of very small amount of oxygen on the particle.
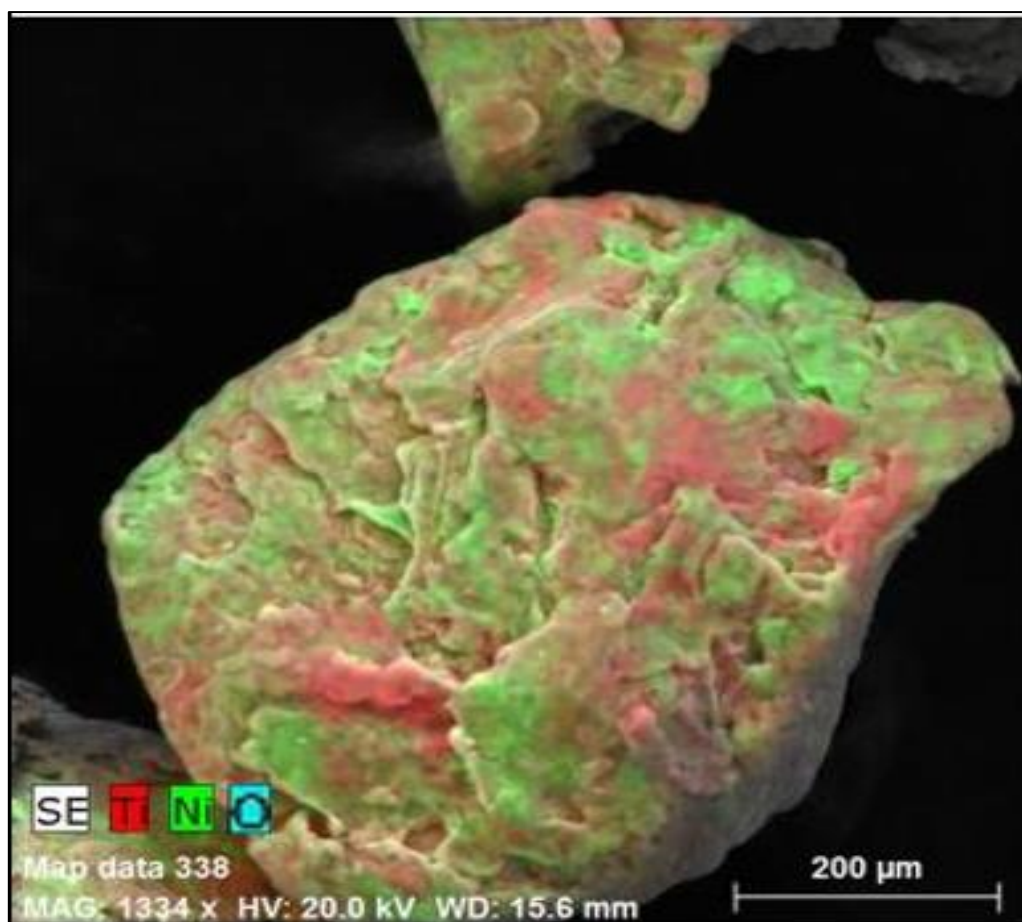
Figure IV.8: Mapping of the distribution of elements on another type of particle after 3 hours of milling.

After 6 hours of milling, begins the appearance of crystalline particles, Figure IV.9 shows the distribution of elements on one of these particles.

We note that the distribution of the elements is much more consistent compared to the other particles that were analyzed for the previous milling times.

It is important to note that the proportion of Fe also increases, which is mainly caused by contamination during milling by the balls and the jar. Fe particles accumulate in groups of about 45 µm [1].
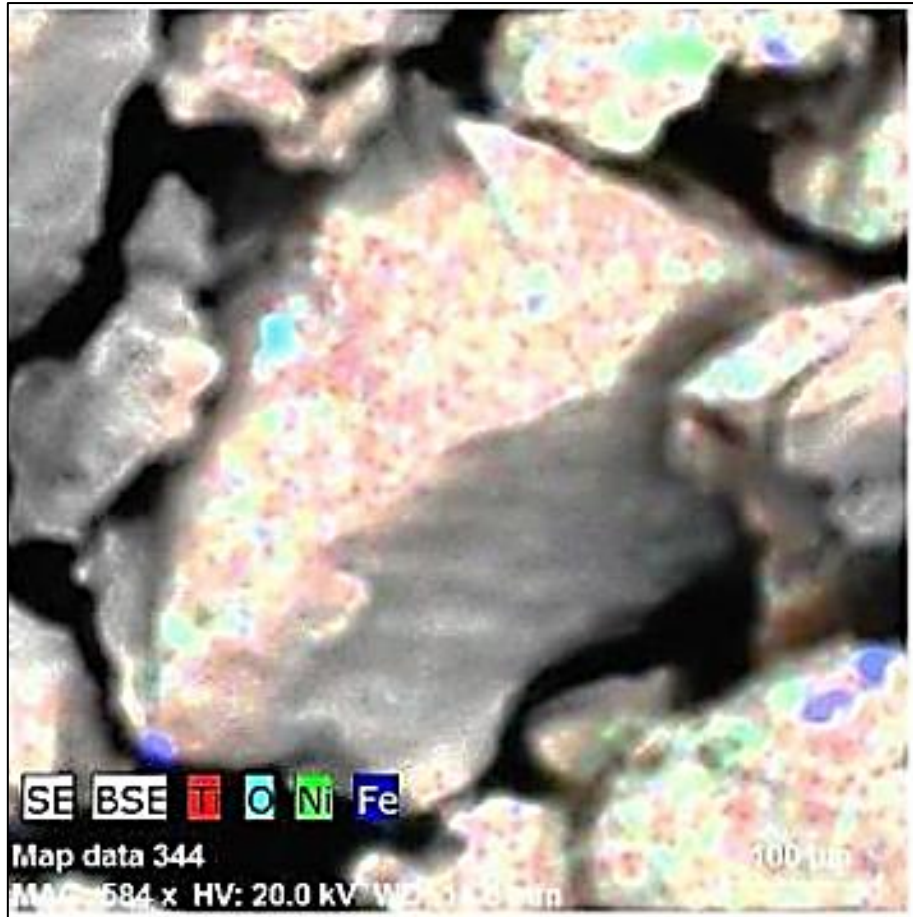
Figure IV.9: Mapping of the distribution of elements on a crystalline particle after 6 hours of milling.

After 12 hours of milling (Figure IV.10), the distribution of Ni and Ti on the powder particles becomes even more consistent. The quantity of O and Fe is increased as indicated in the mapping of each of them and has a size of approximately 10 µm. [7].
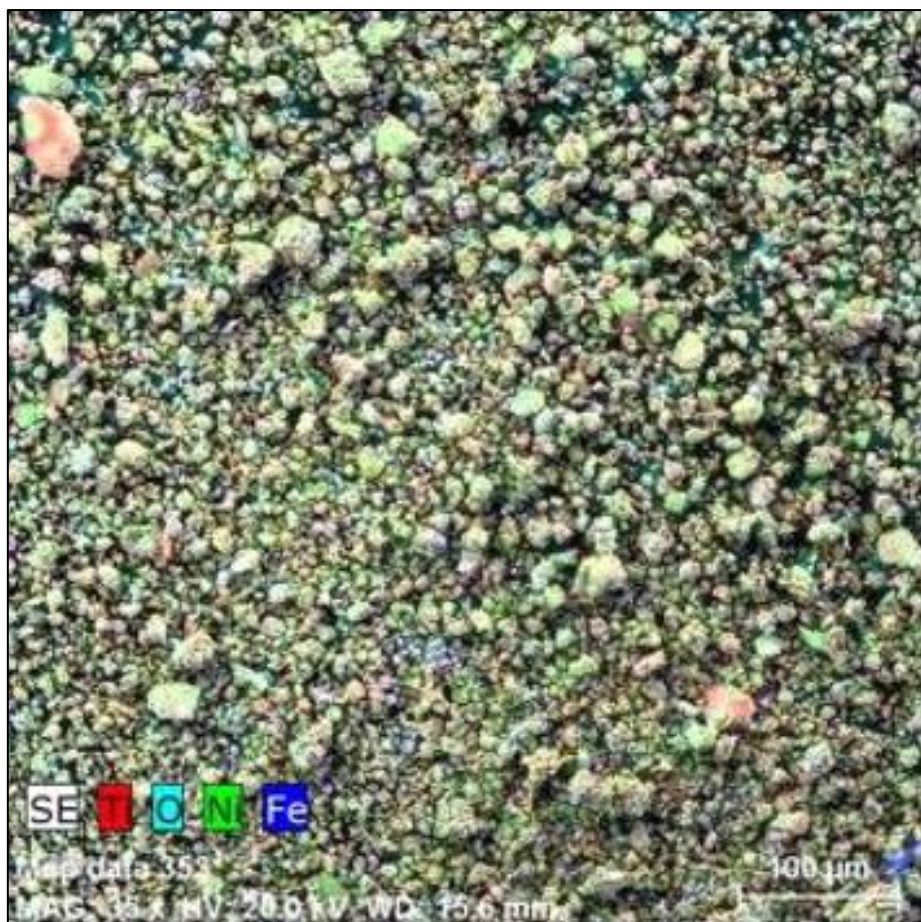
Figure IV.10: Maping of the distribution of $Ni_{50}Ti_{50}$ powder elements after 12 hours of milling.

We show the distribution of elements by cartographic analysis and EDS (Figure IV.11), for a single particle (300 mm) after 12 hours of milling.

The welding effect of the particles is clearly observed, thus forming an almost crystalline particle, which may be the stage before obtaining the crystalline particles.

By studying the EDS spectrum for this region, we note a good distribution of Ni and Ti particles, with quantities of O and Fe of the order of 3.85% and 0.19% respectively (see table IV.1) [6].

Figure IV.11: Mapping of the distribution of elements on a particle after 12 hours of milling.

Elements	Atomic percentage [at. %]
Ni	39.58
Ti	56.48
O	3.85
Fe	0.19

Table IV.1: Proportions of the elements identified by EDS of the aggregates of particles after 12 hours of milling.

References

[1] **Sakher El-fahem**: Thèse doctorat en Physique Elaboration et caractérisation de nanomatériaux à mémoire de forme par mécano synthèse – Département de physique. (2019)

[2] **Montes, J-M F., Cuevas, G., Cintas, J**. : Granular Matter 13:439–446 (2011).

[3] **Loudjani, N., Benchiheub, M., and Bououdina, M**.: J. Supercond Nov. Magn., 29: 2717 (2016).

[4] **Arunkumar, S., Kumaravel, P., Velmurugan, C., Senthilkumar, V**.: International Journal of Minerals, Metallurgy and Materials Volume 25, Number 1, Page 80, (2018).

[5] **Djekoun, A., Otmani, A., Bouzabata, B., Bechiri, L., Randrianantoandro, N., Greneche J.M**. ,Catalysis Today 113:235–239 (2006).

[6] **Lenin, N., Karthik, A., Sridharpanday, M., Selvam, M., Srither, S- R., Arunmetha, S., Paramasivam, P., Rajendran, V**.: Journal of Magnetism and Magnetic Materials 397: 281–286 (2016).

[7] **Alijani, F., Amini, R., Ghaffari, M., Alizadeh, M., Okyay, A-K**.: Materials and Design 55: 373–380 (2014).

General Conclusion

Ni$_{50}$Ti$_{50}$ powder mixtures are made by high-energy milling for milling times of up to 12 hours in a Fritsch "Pulverisette 7" planetary mill from pure elements of nickel and titanium.

The starting powders have a particle size of 45 μm for nickel (99.99% purity), and approximately 150 μm for titanium (99.97% purity). This powder mixture was placed in two sealed packages under an argon atmosphere to prevent oxidation.

Morphological, structural and microstructural changes were followed by scanning electron microscopy (SEM) and EDS.

The morphological contrast study of the powders was followed by the SEM. Before milling the Ni particles, which vary in size from 2 to 110 μm, are characterized by irregular lines, while the dimensions of Ti particles range between 20 and 250 μm, we note that there are two types of Ti particles, most of which have irregular, interlocking and round curved lines.

At the beginning of milling, the powders are flattened. The particle platelets are welded together and form a lamellar structure. As the milling time increases, the spaces between the plates decrease and the defect density increases.

For longer milling times, a true alloy is formed on an atomic scale with the formation of solid solutions, nanocrystalline phases (martensite and austenite) and an amorphous phase.

After analyzing the chemical composition by EDS, it is evident, for the first milling times (1, 3 and 6 h), that the flat particles of Ni and Ti have an irregular distribution.

For milling times of more than 12 hours, the distribution is more homogeneous and uniform. In this case, we concluded that 12 hours of milling was sufficient to obtain a homogeneous Ni$_{50}$Ti$_{50}$ mixture.

Low iron contamination, possibly due to milling tools (balls, jars) was detected by EDS analysis, which accounts for approximately.